HAL
open science

Non-linear eigenvalue problems with GetDP and SLEPc: Eigenmode computations of frequency-dispersive photonic open structures

Guillaume Demésy, André Nicolet, Boris Gralak, Christophe Geuzaine, Carmen Campos, Jose Roman

To cite this version:

Guillaume Demésy, André Nicolet, Boris Gralak, Christophe Geuzaine, Carmen Campos, et al.. Non-linear eigenvalue problems with GetDP and SLEPc: Eigenmode computations of frequency-dispersive photonic open structures. Computer Physics Communications, 2020, 257, pp.107509. 10.1016/j.cpc.2020.107509 . hal-03087303

HAL Id: hal-03087303

https://hal.science/hal-03087303v1

Submitted on 23 Dec 2020

HAL is a multi-disciplinary open access archive for the deposit and dissemination of scientific research documents, whether they are published or not. The documents may come from teaching and research institutions in France or abroad, or from public or private research centers.

L'archive ouverte pluridisciplinaire **HAL**, est destinée au dépôt et à la diffusion de documents scientifiques de niveau recherche, publiés ou non, émanant des établissements d'enseignement et de recherche français ou étrangers, des laboratoires publics ou privés.

arXiv:1802.02363v4 [physics.comp-ph] 1 May 2020

Non-linear eigenvalue problems with GetDP and SLEPc: Eigenmode computations of frequency-dispersive photonic open structures.

Guillaume Demésy[1,*], André Nicolet[1], Boris Gralak[1], Christophe Geuzaine[2], Carmen Campos[3], and Jose E. Roman[3]

[1]Aix Marseille Univ, CNRS, Centrale Marseille, Institut Fresnel, Marseille, France.
[2]University of Liège, Dept. of Electrical Engineering and Computer Science, Montefiore Institute B28, Quartier Polytech 1, Allée de la Découverte 10, B-4000 Liège, Belgium.
[3]Universitat Politècnica de València, D. Sistemes Informàtics i Computació, Camí de Vera, s/n, E-46022 València, Spain.
[*]Corresponding author : `guillaume.demesy@fresnel.fr`.

2020-05-04

Abstract

We present a framework to solve non-linear eigenvalue problems suitable for a Finite Element discretization. The implementation is based on the open-source finite element software GetDP and the open-source library SLEPc. As template examples, we propose and compare in detail different ways to address the numerical computation of the electromagnetic modes of frequency-dispersive objects. This is a non-linear eigenvalue problem involving a non-Hermitian operator. A classical finite element formulation is derived for five different solutions and solved using algorithms adapted to the large size of the resulting discrete problem. The proposed solutions are applied to the computation of the dispersion relation of a diffraction grating made of a Drude material. The important numerical consequences linked to the presence of sharp corners and sign-changing coefficients are carefully examined. For each method, the convergence of the eigenvalues with respect to the mesh refinement and the shape function order, as well as computation time and memory requirements are investigated. The open-source template model used to obtain the numerical results is provided. Details of the implementation of polynomial and rational eigenvalue problems in GetDP are given in appendix.

0 Program Summary

Manuscript title: Non-linear eigenvalue problems with GetDP and SLEPc: Eigenmode computations of frequency-dispersive photonic open structures.
Authors: G. Demésy, A. Nicolet, B. Gralak, C. Geuzaine, C. Campos and J. E. Roman
Program title: NonLinearEVP.pro
Licensing provisions: GNU General Public License 3 (GPL)
Programming language: Gmsh (http://gmsh.info), GetDP (http://getdp.info)

Computer(s) for which the program has been designed: PC, Mac, Tablets, Computer clusters
Operating system(s) for which the program has been designed: Linux, Windows, MacOSX
Keywords: Finite Element Method; Non-linear Eigenvalue Problem; Electromagnetism;
Nature of problem: Computing the eigenvalues and eigenvectors of electromagnetic wave problems involving frequency-dispersive materials. The resulting eigenvalue problem is non-linear and non-hermitian.
Solution method: Finite element method coupled to efficient non-linear eigenvalue solvers: Relevant SLEPc solvers were interfaced to the Finite Element software GetDP. Several linearization schemes are benchmarked.
Running time: From a few seconds for simple problems to several days for large-scale simulations.
References: All appropriate references are contained in the section entitled References.

1 Introduction

The modes of a system are the source free solutions of the propagation equation governing the field behavior in a structured media. They contain all the information regarding the intrinsic resonances of a given structure. In electromagnetism, when dealing frequency-dispersive media, the Helmholtz equation appears as a non-linear eigenvalue problem through the frequency dependence of the permittivities and permeabilities of the involved materials. In general, in wave physics (electromagnetism, acoustics, elasticity...), classical EigenValue Problems (EVPs) become non-linear as soon as a material characteristic property strongly depends on the frequency in the frequency range of interest [1]. We present a general framework to solve non-linear EVPs suitable for a Finite Element (FE) discretization. The implementation is based on the open-source finite element software GetDP and the open-source library SLEPc.

The solutions of such problems may have important applications in electromagnetism at optical frequencies, where frequency dispersion arises in bulk materials. Indeed, the permittivity of most bulk non-transparent materials, such as semiconductors and metals, strongly depends on the excitation frequency [2]. But frequency dispersion also comes into picture when dealing with composites materials, or metamaterials, whose effective electromagnetic parameters derived from modern homogenization schemes [3, 4, 5] are frequency dependent. The accurate and reliable computation of the modes of frequency-dispersive structures represents a great challenge for many applications in nanophotonics.

For smooth and monotonic material dispersion relations, it is possible to think of an iterative process where one would set the permittivity, solve a linear EVP, adjust the permittivity value if necessary, and repeat the process hoping for reasonable convergence for a single eigenvalue... For more tormented dispersion relations, *i.e.* in the vicinity of an intrinsic resonance of a given material, this simple iterative process is very likely to fail. For instance, a direct determination of the spectrum of a 3D gold nanoparticle embedded into a silicon background in the visible range is nowadays extremely challenging.

Fortunately, the relative permittivity function can be accurately described as an analytical function of the frequency. The most famous models are the Drude, Lorentz, Debye models [2], the so-called critical points [6] model or, in general, a rational function of the frequency [7]. In this frame, the non linear EVP becomes rational and can be easily transformed into a polynomial EVP.

In this paper, we numerically investigate various linearization scenarios. We apply these

approaches to an emblematic example in electromagnetism, the study of diffraction gratings. The dispersion relation of a grating is indeed the corner stone of its physical analysis.

The recent literature on modal analysis of such open structures, referred to as Quasi-Normal Modes (QNM), is quite rich. Even if the question of completeness and orthogonality of the QNMs remains open theoretically, numerical quasi-normal modes expansion have been successfully used in various electromagnetic problems, allowing to explain in an elegant manner the resonant mechanisms of a structure and its excitation condition [8, 9]. Their application in nanophotonics can be found in Refs. [8, 10]. As described in the review article in Ref. [11], some numerical approaches already address the problem of the non-linearity of the eigenvalue problem induced by frequency dispersion. A family of "pole search" methods [12, 13, 14] allows to determine eigenvalues one by one by looking for poles of a the determinant of a scattering matrix into the complex plane. Nonetheless, getting the full spectrum in one single computation remains a harsh challenge. Given the spatial nature of the discretization when using FE, the eigenvalue can be factorized in the final assembled matrix system. This fundamental aspect has a fortunate consequence: it is possible to extract all the eigenvalues of the discrete system in one single computation. A Finite Difference Frequency Domain (FDFD) scheme leads to the same property and has been applied recently to open and dispersive electromagnetic structures [15, 16]. It relies on a square Yee grid. Finally, Boundary Elements (BE) have been used [17, 18] to calculate the QNMs of dispersive arbitrarily shaped yet homogeneous structures. Since this method relies on the Green's function, which is eigenfrequency-dependent, a contour integration has to be [18].

We propose to compare several FE schemes to address the non-linear EVP arising from the frequency dispersion. The discrete problem is tackled using recent and efficient algorithms. In the last decade, the numerical analysis community has made significant progress in the numerical solution of non-linear eigenvalue problems, in understanding stability and conditioning issues, and also in proposing effective algorithms. Of particular interest for this paper are iterative methods for computing a few eigenvalues and corresponding eigenvectors of large-scale problems. These kinds of methods have been developed for the case of polynomial eigenvalue problems [19, 20], but also for the more general non-linear case [21]. The latter includes the rational eigenvalue problem, which is indeed relevant for the present case involving a permittivity function explicitly given as a rational function of the eigenvalue. These methods have proved to be effective and some of them are available in the form of robust and efficient implementations in the SLEPc library [22]. With these new solvers, one can routinely compute selected portions of interest of the spectrum of problems with thousands of unknowns on a mere laptop.

The paper is organized as follows. After recalling the mathematical background we present five different approaches to address the non-linearity in the modal problem. For each approach, a variational formulation is derived. These formulations lead to five distinct EVPs: one rational EVP and four polynomial EVPs with various degrees (2, 3 or 4). In a second step, the corresponding discrete problems are numerically benchmarked using the state-of-the-art SLEPc [22] solvers. The issues inherent to the sign-changing coefficients and corners are discussed and the convergence of the fundamental mode of the structure is studied. A discussion on the respective strengths and limitations of all the proposed solutions is conducted. For the purpose of this study, an interface to SLEPc has been implemented in the FE code GetDP [23]. A general description of the implementation of polynomial and rational EVPs in GetDP is given in Appendix III. A template open-source model showing the implementation of each method is provided [24].

2 Problem statement

A practical challenge in computational electromagnetism is the computation, as precise and fast as possible, of many eigenfrequencies of a complicated 3D problem involving frequency-dispersive permittivities and permeabilities. The photonic structure is fully described by two space periodic tensor fields, its relative permittivity $\boldsymbol{\varepsilon}_r(\mathbf{r},\omega)$ and its relative permeability $\boldsymbol{\mu}_r(\mathbf{r})$, where $\mathbf{r} = (x, y, z)$. Note that the permeability tensor is chosen to be non dispersive here because it is the most frequent case when dealing with bulk materials in the optical range. The eigenvalue problem amounts to look for non trivial solutions of the source free Maxwell's equations:

$$\begin{bmatrix} 0 & i(\epsilon_0\boldsymbol{\varepsilon}_r(\mathbf{r},\omega))^{-1}\,\mathbf{curl}\,\cdot \\ -i(\mu_0\boldsymbol{\mu}_r(\boldsymbol{r}))^{-1}\,\mathbf{curl}\,\cdot & 0 \end{bmatrix} \begin{bmatrix} \mathbf{E}(\boldsymbol{r}) \\ \mathbf{H}(\boldsymbol{r}) \end{bmatrix} = \omega \begin{bmatrix} \mathbf{E}(\boldsymbol{r}) \\ \mathbf{H}(\boldsymbol{r}) \end{bmatrix}. \tag{1}$$

Since exploring the possible ways to linearize this problem is a complicated problem in itself, the choice is made to consider a structure as simple as possible and yet highlighting all the difficulties of realistic 3D structures: A mono-dimensional grating made of frequency-dispersive rods, *i.e.* a 2D structure presenting one axis of invariance along z and one direction of periodicity along x. The 2D space variable is from now on denoted by $\boldsymbol{x} := (x, y)$.

Provided that the constitutive tensors of materials have the form

$$\boldsymbol{\varepsilon}_r = \begin{bmatrix} \varepsilon_{xx} & \varepsilon_a & 0 \\ \overline{\varepsilon_a} & \varepsilon_{yy} & 0 \\ 0 & 0 & \varepsilon_{zz} \end{bmatrix} \text{ and } \boldsymbol{\mu}_r = \begin{bmatrix} \mu_{xx} & \mu_a & 0 \\ \overline{\mu_a} & \mu_{yy} & 0 \\ 0 & 0 & \mu_{zz} \end{bmatrix}, \tag{2}$$

the 2D problem can be decoupled into two fundamental polarization cases. They are referred to as s-pol (the electric field is along the axis of invariance) and p-pol (the magnetic field is along the axis of invariance, while the electric field is orthogonal to the axis of invariance). In this paper, the choice is made to focus on the more challenging p-pol case since the s-pol case is easier to tackle [25]. In particular, this polarization case leads to surface plasmons and it is far more representative of the difficulties at stake in the general 3D case.

In the p-pol case, we denote the non vanishing electromagnetic field components by $\mathbf{H} = h(\boldsymbol{x})\,\mathbf{z}$ and $\mathbf{E} = E_x(\boldsymbol{x})\,\mathbf{x} + E_y(\boldsymbol{x})\,\mathbf{y}$. The traditional choice for the unknown in the 2D p-pol case is usually the out-of-plane magnetic field since the problem becomes scalar. Making use of $-\mathbf{curl}\,[\boldsymbol{\varepsilon}_r(\boldsymbol{x},\omega)^{-1}\,\mathbf{curl}\,\mathbf{H}] = \operatorname{div}\left[\boldsymbol{\varepsilon}_r(\boldsymbol{x},\omega)^T/\det(\boldsymbol{\varepsilon}_r(\boldsymbol{x},\omega))\,\mathbf{grad}\,h\right]$, the resulting scalar wave equation writes in absence of electromagnetic source:

$$-\,\mu_{r\,zz}(\boldsymbol{x})^{-1}\operatorname{div}\left[\frac{\boldsymbol{\varepsilon}_r(\boldsymbol{x},\omega)^T}{\det(\boldsymbol{\varepsilon}_r(\boldsymbol{x},\omega))}\,\mathbf{grad}\,h\right] = \frac{\omega^2}{c^2}\,h\,. \tag{3}$$

A less traditional choice for the p-polarization case consists in working with the in-plane electric field $\mathbf{E}$ and the vector wave equation:

$$\boldsymbol{\varepsilon}_r(\boldsymbol{x},\omega)^{-1}\,\mathbf{curl}\,\left[\boldsymbol{\mu}_r^{-1}(\boldsymbol{x})\,\mathbf{curl}\,\mathbf{E}\right] = \frac{\omega^2}{c^2}\,\mathbf{E}\,. \tag{4}$$

What follows is precisely meant to be extended straightforwardly to realistic 3D configurations, where vector fields/edge elements, just as in the 2D vector case, will be at stake. As a consequence, and even though this choice leads to larger problems at the discrete level due to the larger connectivity of edge elements, this vector case is chosen to be the reference problem.

Note that, given the location of the dispersive permittivity in the two wave equations above, it seems more reasonable at first glance to adopt the vector case where $\boldsymbol{\varepsilon}_r(\boldsymbol{x}, \omega)$ is outside the differential operator. As will be shown later, one can arbitrarily choose to consider $\mathbf{E}$ or $\mathbf{H}$ as the unknown of the problem under weak formulation. In fact, the scalar problem in Eq. (3) will be solved as well for enlightening comparison purposes.

The above equations constitute eigenvalue problems where ω^2/c^2 appears as a possible eigenvalue of ω-dependent operators through the ω dependence of the relative permittivity. In other words, modal analysis of frequency-dispersive structures represents a non-linear eigenvalue problem.

3 Opto-geometric characteristics of the model

3.1 Geometry

The formalism presented in this paper is very general in the sense that the tensor fields $\boldsymbol{\varepsilon}_r(\boldsymbol{x}, \omega)$ and $\boldsymbol{\mu}_r(\boldsymbol{x})$ can be defined by part representing the distinct materials of the structure. Several dispersive materials can be considered and modeled by a rational function with an arbitrarily high number of poles. Graded-indexed and fully anisotropic materials can be handled as well.

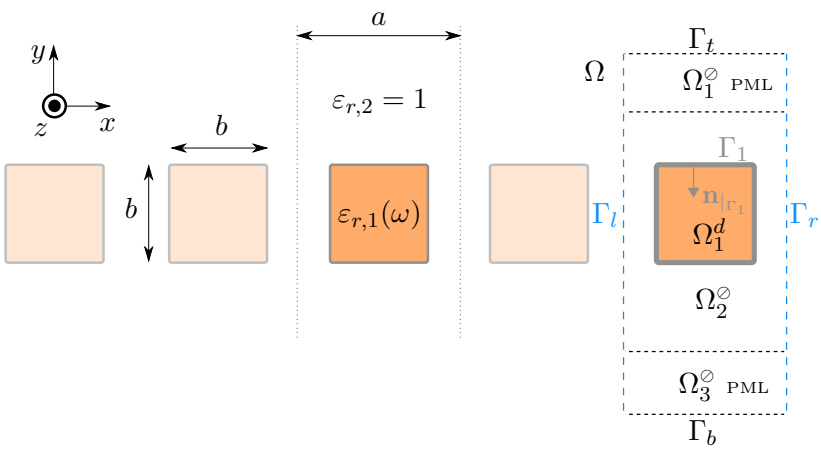

Figure 1: Geometry and notations of the problem.

In spite of the generality of the presented approach, for the sake of clarity, the derivations will be described in the frame of the example described in Fig. 1. We consider from now on a simple free-standing grating with a square section. The structure is periodic along the x axis of period a and invariant along the z-axis. Standard cartesian Perfectly Matched Layers (PMLs [26]) are used to truncate infinite extensions of the domain along the y axis. Let us denote the resulting bounded domain by Ω and its boundary by $\partial\Omega$. The domain Ω can typically be constituted of several dispersive sub-domains with distinct frequency-dispersion relations (in this case, one single rod with support Ω_1^d of boundary Γ_1) and of several non-dispersive sub-domains. All the sub-domains ruled by the same dispersion law can be gathered together since they can be handled all at once. Hence all non-dispersive domains are denoted by $\Omega^{\oslash} = \bigcup_i \Omega_i^{\oslash}$. Finally, for each subset Ω_i, let I_{Ω_i} be its characteristic function: $\mathsf{I}_{\Omega_i}(\boldsymbol{x}) = 1$ if $\boldsymbol{x} \in \Omega_i$ and $\mathsf{I}_{\Omega_i}(\boldsymbol{x}) = 0$ otherwise.

3.2 Material properties

The background is free-space (relative permittivity constant and equal to 1) and the rods are made of a Drude material. Their relative permittivity $\varepsilon_{r,1}$ writes classically [2]:

$$\varepsilon_{r,1}(\omega) = \varepsilon_\infty - \frac{\omega_d^2}{\omega(\omega + i\gamma_d)} \tag{5a}$$

$$= \frac{-\varepsilon_\infty (i\omega)^2 + \varepsilon_\infty \gamma_d (i\omega) - \omega_d^2}{-(i\omega)^2 + \gamma_d (i\omega)} \tag{5b}$$

$$:= \frac{\mathcal{N}_1(i\omega)}{\mathcal{D}_1(i\omega)} \ , \tag{5c}$$

where γ_d, ε_∞ and ω_d are real constants. It is important to note that the Drude model is causal and that $\varepsilon_{r,1}$ is a rational function of $i\omega$ with *real* coefficients (see Eq. (5b)). Finally, more realistic causal models than the Drude model have been found and one can generally write $\varepsilon_{r,1}$ as a rational function (see Eq. (5c), where $\mathcal{N}_1$ and $\mathcal{D}_1$ are polynomial functions of $i\omega$). It would be straightforward to extend this derivation to the more general case involving several frequency-dispersive domains Ω_i^d characterized by their permittivity $\varepsilon_{r,i}(\omega)$ modeled by a causal rational function:

$$\varepsilon_{r,i}(\omega) = \frac{\mathcal{N}_i(i\omega)}{\mathcal{D}_i(i\omega)} = \frac{\sum_{j=1}^{N_i} n_{i,j}\,(i\omega)^j}{\sum_{j=1}^{D_i} d_{i,j}\,(i\omega)^j} \ , \tag{6}$$

where $n_{i,j}$ and $d_{i,j}$ have to be real constants as detailed in Ref. [7].

Finally, the unbounded nature of the problem is handled using PMLs. The reasons for this choice is twofold: (i) from the theoretical point of view, PMLs allow to reveal [27] the so-called Quasi-Normal Modes (PMLs can be regarded as an analytic continuation in the complex plane) and (ii) from the practical point of view, they allow to bound the computational domain (the complex change of variable is encoded into $\boldsymbol{\varepsilon}_r$ and $\boldsymbol{\mu}_r$ resulting in a semi-infinite layer that is eventually truncated).

Discussing the most appropriate PML parameters (*i.e.* damping profile) is outside the scope of this paper, although it would be interesting to apply many of the results obtained in time and time-harmonic domains [28, 29] to the eigenvalue problem. The simplest constant complex stretch ruled by the complex scalar $s_y = a + ib$ is used here. The complex PML tensor is denoted then $\boldsymbol{S} = \mathrm{Diag}(s_y, 1/s_y, s_y)$. One can eventually write the piecewise constant in space and frequency-dependent relative permittivity tensor of the problem as:

$$\boldsymbol{\varepsilon}_r(\boldsymbol{x}, \omega) = \begin{cases} \varepsilon_{r,1}(\omega)\,\boldsymbol{I} & \text{if } \boldsymbol{x} \in \Omega_1^d \\ \varepsilon_{r,2}\,\boldsymbol{I} & \text{if } \boldsymbol{x} \in \Omega_2^\oslash \\ \varepsilon_{r,2}\,\boldsymbol{S} & \text{if } \boldsymbol{x} \in \Omega_1^\oslash \cup \Omega_3^\oslash \end{cases} \ . \tag{7}$$

The piecewise constant relative permeability tensor of the problem writes :

$$\boldsymbol{\mu}_r(\boldsymbol{x}) = \begin{cases} \boldsymbol{I} & \text{if } \boldsymbol{x} \in \Omega_1^d \cup \Omega_2^\oslash \\ \boldsymbol{S} & \text{if } \boldsymbol{x} \in \Omega_1^\oslash \cup \Omega_3^\oslash \end{cases} \ . \tag{8}$$

Finally, Bloch-Floquet theorem is applied to the periodic structure. The problem becomes parametrized by a real scalar α which spans the reduced 1D Brillouin zone $[0, \pi/a]$. In return, the study is restricted to (a, α) quasi-periodic solutions (eigenvectors) of the form $\mathbf{E} = \mathbf{E}_\sharp\, e^{i\alpha x}$, where $\mathbf{E}_\sharp$ is a a-periodic vector field [30].

3.3 Function spaces

Several function spaces are needed to formulate the different approaches of the problem described in the next section.

Concerning the p-pol vector case described in Eq. (4), Bloch boundary conditions [30] are applied on lateral boundaries $\Gamma_l \cup \Gamma_r$. If infinite perfectly matched layers are the appropriate theoretical tool to reveal the quasi-normal modes by rotating the continuous spectrum into the complex plane, they have to be truncated in practice. Truncating the PML discretizes the rotated continuous spectrum and one can choose to apply Dirichlet or Neumann boundary conditions at the bottom of the PML, resulting in a slightly different discretization as detailed in Ref. [27]. We choose homogeneous Dirichlet conditions on $\Gamma_b \cup \Gamma_t$ which decreases the number of unknowns. Let us define the following Sobolev space of (a, α) quasi-periodic vector fields vanishing on $\Gamma_b \cup \Gamma_t$:

$$\boldsymbol{\mathcal{H}}_{\alpha,0}(\Omega, \mathbf{curl}) = \Big\{ \mathbf{E} \in \left(L^2\right)^2 : \mathbf{curl}\,\mathbf{E} \in \left(L^2\right)^2, \\ \mathbf{E} = e^{i\alpha a}\mathbf{E} \text{ and } \mathbf{n}_{|\Gamma_b} \times \mathbf{E} = \mathbf{n}_{|\Gamma_t} \times \mathbf{E} = \mathbf{0} \Big\}. \quad (9)$$

The same considerations apply to the p-pol scalar case described in Eq. (3). However, in order to keep the same discretization of the continuous spectrum, we apply homogeneous Neumann conditions on $\Gamma_b \cup \Gamma_t$. Let us define the following Sobolev space of (a, α) quasi-periodic scalar fields:

$$\boldsymbol{\mathcal{H}}_{\alpha}(\Omega, \mathbf{grad}) = \Big\{ h \in L^2 : \mathbf{grad}\, h \in \left(L^2\right)^2, \\ h_{|\Gamma_r} = e^{i\alpha a} h_{|\Gamma_l} \text{ and } \mathbf{grad}\, h \cdot \mathbf{n}_{|\Gamma_b} = \mathbf{grad}\, h \cdot \mathbf{n}_{|\Gamma_t} = 0 \Big\}. \quad (10)$$

4 Dealing with the eigenvalue problem non-linearity

4.1 A physical linearization via auxiliary fields (Aux-E case)

The problem is reformulated using auxiliary physical fields [31, 32], as detailed in our previous work in Ref. [25]. The procedure to obtain this extension of the Maxwell's classical operator is briefly recalled here. By defining an auxiliary field [33] for each resonance (pole) of the permittivity that couples with classical electromagnetic fields, one can extend and linearize the classical Maxwell operator. In the present case of a simple Drude model recalled in Eq. (5a), a single auxiliary field denoted $\boldsymbol{A}_1^d$ is required, and defined in frequency-domain as:

$$\boldsymbol{A}_1^d(\boldsymbol{x}, t) = -2i\frac{\omega_d}{\sqrt{2}} \int_{-\infty}^{t} \exp[-\gamma_d(t-s)]\, \mathbf{E}(\boldsymbol{x}, s)\, \mathrm{d}s. \quad (11)$$

This auxiliary field $\boldsymbol{A}_1^d$ has for spatial support Ω_1^d and satisfies natural boundary conditions on Γ_1. It belongs to $\boldsymbol{\mathcal{H}}(\Omega_1^d, \mathbf{curl})$. An intermediate frequency-dispersion free permittivity tensor field $\boldsymbol{\varepsilon}_r^{\oslash}(\boldsymbol{x})$ is convenient here:

$$\boldsymbol{\varepsilon}_r^{\oslash}(\boldsymbol{x}) = \begin{cases} \varepsilon_\infty \boldsymbol{I} & \text{if } \boldsymbol{x} \in \Omega_1^d \\ \varepsilon_{r,2} \boldsymbol{I} & \text{if } \boldsymbol{x} \in \Omega_2^{\oslash} \\ \varepsilon_{r,2} \boldsymbol{S} & \text{if } \boldsymbol{x} \in \Omega_1^{\oslash} \cup \Omega_3^{\oslash} \end{cases}. \quad (12)$$

In matrix form, the following linear eigenvalue problem is obtained:

$$\boldsymbol{M}(\boldsymbol{x})\,\mathcal{U}(\boldsymbol{x}) = \omega\,\mathcal{U}(\boldsymbol{x})\,, \tag{13}$$

where $\mathcal{U}(\boldsymbol{x}) = [\mathbf{E}(\boldsymbol{x}), \mathbf{H}(\boldsymbol{x}), \boldsymbol{A}_1^d(\boldsymbol{x})]^T$ and

$$\boldsymbol{M}(\boldsymbol{x}) = \begin{bmatrix} 0 & i(\epsilon_0\boldsymbol{\varepsilon}_r^{\oslash})^{-1}\,\mathbf{curl}\,\cdot & \dfrac{\omega_d}{\sqrt{2}}\boldsymbol{\varepsilon}_r^{\oslash\,-1} \\ -i(\mu_0\boldsymbol{\mu}_r)^{-1}\,\mathbf{curl}\,\cdot & 0 & 0 \\ 2\dfrac{\omega_d}{\sqrt{2}} & 0 & -i\gamma_d \end{bmatrix}. \tag{14}$$

Note that when discretizing the problem using FE, the electric field and magnetic field cannot be represented on the same edges. The former should be discretized on the dual basis of the latter. However, the basis functions associated with the dual unstructured FEM mesh are not easy to construct. A possible workaround would consist in working with face elements and the 2-form $\mathbf{B}$ instead of edge elements and the 1-form $\mathbf{H}$. Alternatively, in this paper, we classically chose to eliminate $\mathbf{H}$. The cost is that a quadratic eigenproblem is obtained whereas the system in Eq. (14) was linear:

$$\omega^2\,\boldsymbol{M}_2(\boldsymbol{x})\,\mathcal{V}(\boldsymbol{x}) + \omega\,\boldsymbol{M}_1(\boldsymbol{x})\,\mathcal{V}(\boldsymbol{x}) + \boldsymbol{M}_0(\boldsymbol{x})\,\mathcal{V}(\boldsymbol{x}) = \mathbf{0}\,, \tag{15}$$

where $\mathcal{V}(\boldsymbol{x}) = [\mathbf{E}(\boldsymbol{x}), \boldsymbol{A}_1^d(\boldsymbol{x})]^T$ and

$$\boldsymbol{M}_2 = \begin{bmatrix} -\boldsymbol{\varepsilon}_r^{\oslash} & 0 \\ 0 & 0 \end{bmatrix},\ \boldsymbol{M}_1 = \begin{bmatrix} 0 & \dfrac{\omega_d}{\sqrt{2}} \\ 0 & -1 \end{bmatrix},\ \boldsymbol{M}_0 = \begin{bmatrix} c^2\,\mathbf{curl}\,[\boldsymbol{\mu}_r^{-1}\,\mathbf{curl}\,\cdot] & 0 \\ 2\dfrac{\omega_d}{\sqrt{2}} & -i\gamma_d \end{bmatrix}. \tag{16}$$

Finally, this quadratic eigenvalue problem writes under variational form:

$$\left|\begin{array}{l} \text{Given } \alpha \in [0, \pi/a], \\ \text{find } (\omega, \left[\mathbf{E}, \boldsymbol{A}_1^d\right]^T) \in \mathbb{C} \times \left[\boldsymbol{\mathcal{H}}_{\alpha,0}(\Omega, \mathbf{curl}) \times \boldsymbol{\mathcal{H}}(\Omega_1^d, \mathbf{curl})\right] \text{ such that:} \\ \quad \forall \mathcal{W} = \left[\mathbf{W}\,,\,\mathbf{W}_a\right] \in \boldsymbol{\mathcal{H}}_{\alpha,0}(\Omega, \mathbf{curl}) \times \boldsymbol{\mathcal{H}}(\Omega_1^d, \mathbf{curl}), \\ \qquad \omega^2 \displaystyle\int_\Omega (\boldsymbol{M}_2\mathcal{V})\,\overline{\mathcal{W}}\,\mathrm{d}\Omega + \omega \int_\Omega (\boldsymbol{M}_1\mathcal{V})\,\overline{\mathcal{W}}\,\mathrm{d}\Omega + \int_\Omega (\boldsymbol{M}_0\mathcal{V})\,\overline{\mathcal{W}}\,\mathrm{d}\Omega = 0. \end{array}\right. \tag{17}$$

This linearization can be described as a physical one since, unlike the purely numerical ones in the following, a larger system is obtained with extra unknowns *inside the dispersive element solely.* In this simplified version of the auxiliary fields theory called the resonance formalism, the auxiliary field fulfills a simple relation with the polarization vector: $\partial_t\mathbf{P}(\boldsymbol{x}, t) = i\epsilon_0\frac{\omega_d}{\sqrt{2}}\boldsymbol{A}_1^d(\boldsymbol{x}, t)$. This approach is identical to the one presented by Fan *et al.* in Ref. [34]. It is also very similar to the treatment of frequency-dispersive media made in time domain methods for direct problems such as FDTD [35].

In the following, the case described in Eq. (17) will be referred to as the Aux-E case.

4.2 Electric field polynomial eigenvalue problem (PEP-E and NEP-E cases)

In this section, a purely numerical linearization is considered. This approach begins with writing the eigenvalue problem Eq. (4) under its variational form:

$$\left|\begin{array}{l}\text{Given } \alpha \in [0, \pi/a], \text{ find } (\omega, \mathbf{E}) \in \mathbb{C} \times \boldsymbol{\mathcal{H}}_{\alpha,0}(\Omega, \mathbf{curl}) \text{ such that:} \\ \quad \forall\, \mathbf{W} \in \boldsymbol{\mathcal{H}}_{\alpha,0}(\Omega, \mathbf{curl}), \\ \qquad -\displaystyle\int_\Omega \boldsymbol{\mu}_r^{-1}\, \mathbf{curl}\, \mathbf{E} \cdot \overline{\mathbf{curl}\, \mathbf{W}}\, \mathrm{d}\Omega + \frac{\omega^2}{c^2} \int_\Omega \boldsymbol{\varepsilon}_r(\boldsymbol{x}, \omega)\, \mathbf{E} \cdot \overline{\mathbf{W}}\, \mathrm{d}\Omega = 0\,.\end{array}\right. \tag{18}$$

Note that the boundary term on periodic lines Γ_r and Γ_l vanishes due to opposite signs of normals [36].

Then, recalling that the whole domain Ω can be split into frequency-dispersive domains (Ω_1^d solely in this simplified case) and non dispersive domains $\Omega^\oslash$, and that the permittivity tensor is a constant by part tensor field of $\boldsymbol{r}$, the problem becomes :

$$\left|\begin{array}{l}\text{Given } \alpha \in [0, \pi/a], \text{ find } (\omega, \mathbf{E}) \in \mathbb{C} \times \boldsymbol{\mathcal{H}}_{\alpha,0}(\Omega, \mathbf{curl}) \text{ such that:} \\ \quad \forall\, \mathbf{W} \in \boldsymbol{\mathcal{H}}_{\alpha,0}(\Omega, \mathbf{curl}), \\ \qquad -\displaystyle\int_\Omega \boldsymbol{\mu}_r^{-1}\, \mathbf{curl}\, \mathbf{E} \cdot \overline{\mathbf{curl}\, \mathbf{W}}\, \mathrm{d}\Omega \\ \qquad + \dfrac{\omega^2}{c^2} \displaystyle\int_{\Omega^\oslash} \boldsymbol{\varepsilon}_r^\oslash\, \mathbf{E} \cdot \overline{\mathbf{W}}\, \mathrm{d}\Omega + \frac{\omega^2}{c^2} \frac{\mathcal{N}_1(i\omega)}{\mathcal{D}_1(i\omega)} \int_{\Omega_1^d} \mathbf{E} \cdot \overline{\mathbf{W}}\, \mathrm{d}\Omega = 0\,.\end{array}\right. \tag{19}$$

A last mere multiplication by $\mathcal{D}_1(i\omega)$ allows to express the problem under the form of a polynomial eigenvalue problem:

$$\left|\begin{array}{l}\text{Given } \alpha \in [0, \pi/a], \text{ find } (\omega, \mathbf{E}) \in \mathbb{C} \times \boldsymbol{\mathcal{H}}_{\alpha,0}(\Omega, \mathbf{curl}) \text{ such that:} \\ \quad \forall\, \mathbf{W} \in \boldsymbol{\mathcal{H}}_{\alpha,0}(\Omega, \mathbf{curl}), \\ \qquad -\mathcal{D}_1(i\omega) \displaystyle\int_\Omega \boldsymbol{\mu}_r^{-1}\, \mathbf{curl}\, \mathbf{E} \cdot \overline{\mathbf{curl}\, \mathbf{W}}\, \mathrm{d}\Omega \\ \qquad + \dfrac{\omega^2}{c^2} \mathcal{D}_1(i\omega) \displaystyle\int_{\Omega^\oslash} \boldsymbol{\varepsilon}_r^\oslash\, \mathbf{E} \cdot \overline{\mathbf{W}}\, \mathrm{d}\Omega + \frac{\omega^2}{c^2} \mathcal{N}_1(i\omega) \int_{\Omega_1^d} \mathbf{E} \cdot \overline{\mathbf{W}}\, \mathrm{d}\Omega = 0.\end{array}\right. \tag{20}$$

The Drude permittivity model has a pole in zero, leading to a polynomial EVP of order 3. Otherwise, when considering one single frequency-dispersive material, the final order will be $2+\mathrm{Deg}(\mathcal{D}_i)$. More generally, note that the final degree of the polynomial EVP is $2+\sum_{i=1}^N \mathrm{Deg}(\mathcal{D}_i)$ in the case of N (distinct) frequency-dispersive materials.

In the following, the approaches described in Eq. (20) and Eq. (19) will be referred to as the PEP-E and NEP-E approaches respectively (resp.). They differ by the type of solver used for their numerical treatment as detailed later.

4.3 Electric field polynomial eigenvalue problem with Lagrange multipliers (Lag-E case)

One can consider the polynomial eigenvalue problem under its strong form, by a mere multiplication of the propagation equation by the denominator of the frequency-dispersive permittivity.

Recalling that the relative permittivity tensor field is defined by part in each domain, we obtain:

$$\left(\mathsf{I}_{\Omega^\oslash}(\boldsymbol{x}) + \mathcal{D}_1(i\omega)\,\mathsf{I}_{\Omega_1^d}(\boldsymbol{x})\right)\mathbf{curl}\,\left[\boldsymbol{\mu}_r^{-1}(\boldsymbol{x})\,\mathbf{curl}\,\mathbf{E}\right] = \left(\boldsymbol{\varepsilon}_r(\boldsymbol{x})\,\mathsf{I}_{\Omega^\oslash} + \mathcal{N}_1(i\omega)\mathsf{I}_{\Omega_1^d}(\boldsymbol{x})\right)\frac{\omega^2}{c^2}\,\mathbf{E}\,. \quad (21)$$

Terms of the form $[f(\boldsymbol{x})\,\mathbf{curl}\,\boldsymbol{\mu}_r^{-1}\mathbf{curl}\,\mathbf{E}]$ are obtained, where f is a constant by part complex scalar function. The weak formulation is not classical, since after multiplication by a test function $\mathbf{W}$ and integration over Ω, we obtain in the sense of distributions :

$$\begin{aligned}\int_\Omega \left[f(\mathbf{x})\,\mathbf{curl}\,\boldsymbol{\mu}_r^{-1}\mathbf{curl}\,\mathbf{E}\right]\cdot\overline{\mathbf{W}}\,\mathrm{d}\Omega = &\int_\Omega f(\mathbf{x})\,\boldsymbol{\mu}_r^{-1}\,\mathbf{curl}\,\mathbf{E}\cdot\mathbf{curl}\,\overline{\mathbf{W}}\,\mathrm{d}\Omega\\ &-\int_{\partial\Omega} f(\mathbf{x})\,\left[\boldsymbol{\mu}_r^{-1}\,\mathbf{curl}\,\mathbf{E}\times\mathbf{n}_{|\partial\Omega}\right]\cdot\overline{\mathbf{W}}\,\mathrm{d}\Gamma\\ &+\int_{\Gamma_1} f_{\text{jump}}^{\oslash\to d}\left[\left[\boldsymbol{\mu}_r^{-1}\,\mathbf{curl}\,\mathbf{E}\right]\times\mathbf{n}_{|\Gamma_1}\right]\cdot\overline{\mathbf{W}}\,\mathrm{d}\Gamma\,,\end{aligned} \quad (22)$$

where $f_{\text{jump}}^{\oslash\to d}$ is the jump of f across Γ_1. The two first terms in the right hand side of Eq. (22) are exactly like those arising from the traditional integration by part of the **curl** (pondered by f). As for the last term, it represents a jump to enforce the quantity $\left[[\boldsymbol{\mu}_r^{-1}\,\mathbf{curl}\,\mathbf{E}]\times\mathbf{n}_{|\Gamma_1}\right]$, which is nothing but the tangential trace of $\boldsymbol{\mu}_r^{-1}\,\mathbf{curl}\,\mathbf{E}$ on Γ_1. This quantity is not readily accessible and requires the adjunction of a Lagrange multiplier. In other words, the procedure now consists in splitting the problem into groups ruled by the same frequency dispersion law and introducing an extra unknown in order to reassemble the different groups while satisfying the appropriate fields discontinuities. Thus, the problem is split into two distinct parts and two fields $\mathbf{E}_1$ and $\mathbf{E}_2$ are defined, with respective support Ω_1^d and $\Omega^\oslash$. A Lagrange multiplier $\boldsymbol{\lambda}$ is introduced on Γ_1 in order to set the appropriate boundary conditions. It remains to define the appropriate trace space of Ω_1^d on Γ_1 [37]: $\boldsymbol{\mathcal{H}}^{-1/2}(\mathrm{div},\Gamma_1) = \{\mathbf{u}\times\mathbf{n}_{|\Gamma_1} : \mathbf{u}\in\mathcal{H}(\mathbf{curl},\Omega_1)\}$ which coincides with the trace space of $\Omega^\oslash$ on Γ_1 up to the orientation of the normals.

The variational form of the eigenproblem writes:

Given $\alpha\in[0,\pi/a]$, find $(\omega,(\mathbf{E}_1,\mathbf{E}_2,\boldsymbol{\lambda}))\in$
$\mathbb{C}\times\left[\boldsymbol{\mathcal{H}}(\Omega_1^d,\mathbf{curl})\times\boldsymbol{\mathcal{H}}_{\alpha,0}(\Omega^\oslash,\mathbf{curl})\times\boldsymbol{\mathcal{H}}^{-1/2}(\mathrm{div},\Gamma_1)\right]$ such that:
$\forall\,[\mathbf{W}_1,\mathbf{W}_2,\boldsymbol{\nu}]^T\in$
$\boldsymbol{\mathcal{H}}(\Omega_1^d,\mathbf{curl})\times\boldsymbol{\mathcal{H}}_{\alpha,0}(\Omega^\oslash,\mathbf{curl})\times\boldsymbol{\mathcal{H}}^{-1/2}(\mathrm{div},\Gamma_1)$,

- $$\mathcal{D}_1(i\omega)\int_{\Omega_1^d}\boldsymbol{\mu}_r^{-1}\mathbf{curl}\,\mathbf{E}_1\cdot\overline{\mathbf{curl}\,\mathbf{W}_1}\,\mathrm{d}\Omega + \frac{\omega^2}{c^2}\mathcal{N}_1(i\omega)\int_{\Omega_1^d}\mathbf{E}_1\cdot\overline{\mathbf{W}_1}\,\mathrm{d}\Omega + \mathcal{D}_1(i\omega)\int_{\Gamma_1}\boldsymbol{\lambda}\cdot\overline{\mathbf{W}_1}\,\mathrm{d}\Gamma = 0 \quad (23a)$$
- $$\int_{\Omega^\oslash}\boldsymbol{\mu}_r^{-1}\mathbf{curl}\,\mathbf{E}_2\cdot\overline{\mathbf{curl}\,\mathbf{W}_2}\,\mathrm{d}\Omega + \frac{\omega^2}{c^2}\int_{\Omega^\oslash}\boldsymbol{\varepsilon}_r^\oslash\,\mathbf{E}_2\cdot\overline{\mathbf{W}_2}\,\mathrm{d}\Omega - \int_{\Gamma_1}\boldsymbol{\lambda}\cdot\overline{\mathbf{W}_2}\,\mathrm{d}\Gamma = 0 \quad (23b)$$
- $$\int_{\Gamma_1}\mathbf{n}_{|\Gamma_1}\times(\mathbf{E}_1+\mathbf{E}_2)\cdot\overline{\boldsymbol{\nu}}\,\mathrm{d}\Gamma = 0\,. \quad (23c)$$

In the system Eqs. (23), the two first equations Eqs. (23a, 23b), apart from their respective last boundary term, are nothing but the variational form of the wave equation in the dispersive domain Ω_1^d (Eq. (23a)) and in the non-dispersive domain $\Omega^{\oslash}$. As for this last boundary term, it accounts for the discontinuity of the denominator of the permittivity over Ω through the Lagrange multiplier $\boldsymbol{\lambda}$ by imposing appropriate jumps to the tangential trace of $\boldsymbol{\mu}_r^{-1}\,\mathbf{curl}\,\mathbf{E}$ on Γ_1. Finally, the continuity of the tangential component of $\mathbf{E} = \mathbf{E}_1 + \mathbf{E}_2$ on Γ_1 is restored in Eq. (23c).

The advantage of this approach is that, in case of several dispersive materials, the degree of the final polynomial EVP remains $\mathrm{Max}_i\{\mathrm{Deg}(\mathcal{D}_i), 2 + \mathrm{Deg}(\mathcal{N}_i)\}$ instead of being the sum of the degrees the $\mathcal{D}_i$ polynomials as in Sec. 4.2. However, in this example where a Drude material is in contact with a dispersion-free region, it results in a 3rd order polynomial as in the PEP-E approach. Note that one drawback is the additional surface unknowns introduced by the Lagrange multipliers.

In the following, the approach described by Eqs. (23a,23b,23c) will be referred to as the Lag-E approach.

4.4 Magnetic field polynomial eigenvalue problem (PEP-h case)

For reference and comparison, we will also solve here the scalar problem corresponding to Eq. (3). Let us recall that homogeneous Neumann boundary conditions are imposed at the extremities of the PMLs in order to keep the same discretization of the continuous spectrum as in the other approaches based on the electric field. This continuous scalar problem can be tackled using nodal elements whereas the previous ones requires edge elements. The same considerations as in the previous vector case allow to establish the eigenproblem for the scalar unknown h:

$$\left|\begin{array}{l}\text{Given } \alpha \in [0, \pi/a], \text{ find } (\omega, h) \in \mathbb{C} \times \boldsymbol{\mathcal{H}}_{\alpha,0}(\Omega, \mathbf{grad}) \text{ such that:}\\ \quad \forall w \in \boldsymbol{\mathcal{H}}_{\alpha,0}(\Omega, \mathbf{grad}),\\ \qquad -\mathcal{D}_1(i\omega)\displaystyle\int_{\Omega_1^d} \mathbf{grad}\, h \cdot \overline{\mathbf{grad}\, w}\,\mathrm{d}\Omega\\ \qquad -\mathcal{N}_1(i\omega)\displaystyle\int_{\Omega^{\oslash}} \frac{\boldsymbol{\varepsilon}_r(\boldsymbol{x})^T}{\det(\boldsymbol{\varepsilon}_r(\boldsymbol{x}))}\,\mathbf{grad}\, h \cdot \overline{\mathbf{grad}\, w}\,\mathrm{d}\Omega\\ \qquad +\dfrac{\omega^2}{c^2}\mathcal{N}_1(i\omega)\displaystyle\int_{\Omega} \mu_{rzz}\, h \cdot \overline{w}\,\mathrm{d}\Omega = 0\,.\end{array}\right. \tag{24}$$

In the present grating example with a Drude material, it results in a 4th order polynomial EVP.

In the following, the approach described in Eq. (24) will be referred to as the PEP-h approach.

5 Solving the discrete problem

5.1 Discretization and summary

The structure described in Fig. 1 was meshed using the open source mesh generator Gmsh [38]. A sample mesh is shown in Fig. 2. In the following numerical experiments, the distance from the object to the PML is set to a and the PML thickness to $3a$. The mesh size is set to a/N

in $\Omega_2^{\oslash}$ (free-space), $a/(3N)$ in and around Ω_1^d (dispersive rod), where N is set to an integer value. Note that this last value of the mesh refinement in the dispersive rod is arbitrary since its permittivity is eigenvalue-dependent. Indeed one cannot choose the mesh size like in time-harmonic direct problems: In direct cases, the frequency is fixed, and thus the spatial variations characteristic length of the unknown field inside each domain are known in advance. As will be discussed in Sec. 6.2, the mesh is globally unstructured and locally structured in order to be symmetric at the interface with the dispersive material. Finally, the mesh is periodic in the direction of periodicity of the grating.

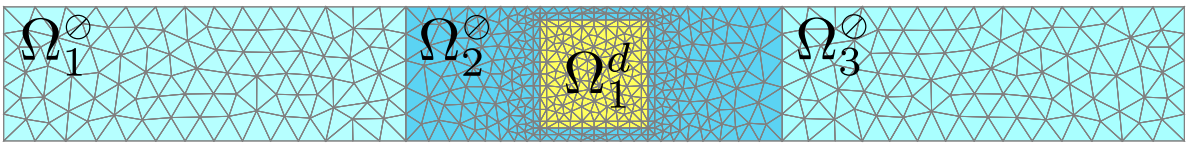

Figure 2: Mesh of the computational domain for $N = 5$. The mesh size is set to a/N in $\Omega_2^{\oslash}$ (free-space), $a/(2N)$ in and around Ω_1^d (dispersive rod).

First or second order edge elements (or Webb elements with interpolation order $k = 1$ or 2 [39, 40]) are used in electric field cases (Aux-E, PEP-E, NEP-E, Lag-E) and first or second order nodal elements are used in the magnetic field case (PEP-h) depending on the study. The GetDP [23] software allows to handle the various required basis functions handily (details about the implementation are given in Appendix III). Finally, ONELAB is an open-source software bundle [41], containing both Gmsh and GetDP, which provides a lightweight graphical interface to these programs. A ONELAB open-source model can be downloaded from [24] and allows to reproduce the results presented in Sec. 6.5.

The different cases and their main differences (unknown field, polynomial orders, number of DOFs for a particular mesh, solver used) are summed up in Table 1.

Table 1: A synthetic view of all the presented approaches.

Name	Aux-E	PEP-E	NEP-E	Lag-E	PEP-h
Formulation	Eq. (17)	Eq. (20)	Eq. (19)	Eq. (23)	Eq. (24)
Unknown(s)	$\mathbf{E}$, $\boldsymbol{A}_1^d$	$\mathbf{E}$	$\mathbf{E}$	$\mathbf{E}_1$, $\mathbf{E}_2$, $\boldsymbol{\lambda}$	h
Element type	Edge	Edge	Edge	Edge	Nodal
Polynomial order	2	3	(rational)	3	4
SLEPc solver	PEP	PEP	NEP	PEP	PEP
Number of DOFs	44596	34150	34150	34750	23688

5.2 Solvers

Very recent progress in sparse matrix eigenvalue solvers allow to tackle the discrete problem very efficiently. For the purpose of this study, we interfaced GetDP with two particularly well suited and recent solvers of the SLEPc library [22] dedicated to solve large scale sparse eigenvalue problems. Depending on the eigenproblem, GetDP can call linear, quadratic, general polynomial, or rational eigenvalue solvers of SLEPc[1].

Concerning the auxiliary field (Aux-E) formulation, all is needed is a solver adapted to quadratic eigenproblems. Again, that is the particularity of this physical linearization, one can

[1] A version of SLEPc 3.8.0 or more recent is required.

add more poles to the permittivity rational function or more dispersive materials: It will only result in defining new auxiliary fields in the elements leading to a larger system that will remain quadratic.

As for the polynomial eigenproblems (PEP-E, Lag-E, PEP-h) described in Eqs. (20,23,24), the matrices corresponding to the various powers of ω (that is, in the reference example, 4 matrices for the electric field formulations and 5 for the magnetic electric field formulation) are assembled separately in GetDP and simply passed to SLEPc. SLEPc provides a PEP module for the solution of polynomial eigenvalue problems, either quadratic or of higher degree d. The user can choose among several solvers. Most of these solvers are based on linearization, meaning that internally a linear eigenvalue problem is built somehow and solved with more traditional linear eigensolvers. The linear eigenproblem produced by the linearization is of dimension $d \cdot n$, where n is the size of the polynomial problem. Hence, a naive implementation of the linearization is going to require d times as much memory with respect to the linear case. The default SLEPc polynomial solver, named TOAR, is memory-efficient because it represents the subspace basis in a compact way, $V = (I_d \otimes U)G$, where vectors of the basis U have length n as opposed to length $d \cdot n$ for vectors of V. The TOAR algorithm builds a Krylov subspace with this basis structure, and it has been shown to be numerically stable [42]. Apart from the memory savings, the method is cheaper in terms of computations compared to operating with the explicitly formed linearization. In particular, when performing the shift-and-invert spectral transformation for computing eigenvalues close to a given target value in the complex plane, it is not necessary to factorize a matrix of order $d \cdot n$ but a matrix of order n instead. SLEPc's solvers also incorporate all the necessary ingredients for making the method effective and accurate, such as scaling, restart, eigenvalue locking, eigenvector extraction, and iterative refinement, as well as parallel implementation. All the details can be found in [43].

The rational eigenproblem described in Eq. (19) is even simpler since SLEPc now has a built-in solver class to handle complex rational functions. As a result, one can directly provide the 3 necessary matrices corresponding to the tree terms in Eq. (19), along with the desired dispersive relative permittivity function. Note that for several dispersive domains with distinct materials with a high number of poles, the product of all the involved denominators in the polynomial approach (Eq. (20)) would be tedious to write. However, the number of terms to write with the NEP solvers remains "two plus the number of distinct dispersive media". We present both these twin approaches, but, from the practical point of view, the rational NEP solver class is clearly the best match for the purpose of this study.

SLEPc's NEP module for general non-linear eigenproblems [44] can be used to compute a few eigenvalues (and corresponding eigenvectors) of any eigenproblem that is non-linear with respect to the eigenvalue (not the eigenvector). This includes the rational eigenvalue problem, for which SLEPc solvers provide specific support. The problem is expressed in the form

$$\sum_{i=0}^{\ell-1} A_i f_i(\lambda) x = 0, \tag{25}$$

where A_i are the matrix coefficients and $f_i(\cdot)$ are non-linear functions. Again, SLEPc provides a collection of solvers from which the user can select the most appropriate one. Particularly interesting are the methods based on approximation followed by linearization. An example of such methods is the interpolation solver, that approximates the non-linear function by the interpolation polynomial in a given interval, and then uses the PEP module to solve the resulting polynomial eigenproblem. This approach is available only for the case of real eigenvalues

and hence cannot be applied to this case. A similar strategy is used in the NLEIGS algorithm [45], that builds a rational interpolation which in turn is linearized to get a linear eigenvalue problem. As opposed to the case of the polynomial eigenproblem, in this case the dimension of the linearized problem is not known a priori, since the number of terms depends on the function being interpolated. NLEIGS determines the number of terms based on a tolerance for interpolation. In a general non-linear function, the user must provide a discretization of the singularity set, but in the case that the non-linear eigenproblem is itself rational, this is not necessary and SLEPc automatically builds an exact rational interpolation of size equal to the number of poles (plus the degree of the polynomial part if present). Once the rational interpolation is obtained, the last step is to create a memory-efficient Krylov expansion associated with the linearization, in a similar way as in polynomial problems, without explicitly building the matrix of the linearization and representing the Krylov basis in a compact way. This is the approach that has been used in this paper for the NEP-E formulation.

6 Spectrum of the dispersive grating

The numerical values used in Refs. [12, 25] in the case of 2D photonic crystals are considered here:

$$\varepsilon_\infty = 1,\ \gamma_d = 0.05\eta,\ \text{and}\ \omega_d = 1.1\eta,\ \text{with}\ \eta = \frac{2\pi c}{a}. \tag{26}$$

The square rod section is set to $b = 0.806a$. For the spectra computed in this section, second order FE shape functions are used and the mesh parameter is set to $N = 8$ (cf. Fig. 2).

6.1 Dispersion relation in the complex plane

For each formulation, the reduced Brillouin zone $[0, \pi/a]$ is sampled by 60 points. For each value of the Bloch variable α, 500 complex eigenvalues are computed inside a predefined rectangular region of interest in the lower right quarter of the complex plane.

This set of eigenvalues forms the dispersion relation of the grating for which a standard representation (ω against α) is given in Appendix I. Choosing a representation in the complex frequency plane brings an enlightening viewpoint. Indeed, the lower right quarter of the complex plane of interest (positive real part, negative imaginary part corresponding to a damping in time) exhibits several very particular and unavoidable points. The dispersion relations for all five problems are represented in the complex plane in Fig. 3(a). The parameter in color scale is the Bloch variable α. Horizontal "_" and vertical "|" hyphens represent the eigenvalues of the QNMs of interest for the electric and magnetic field formulations respectively. A selection of eigenvectors computed using the PEP-h formulation is given in Figs. 3(b-i).

As detailed in Appendix I, the PML modes (represented here by grey dots, with eigenfields confined in the PMLs, see h_6 in Fig. 3(g)) can be numerically distinguished from QNMs using a twofold criterion. It is stressed that each colored curve in the complex plane is a photonic band of the grating. For more physical considerations about these bands, one can refer to [46]. The most commonly used are the low frequency ones (close to the real line as h_5 or h_2 in Figs. 3(f,c)).

The first striking point is the perfect numerical agreement between all the approaches based on the electric field (colored horizontal bars "_"). It is as good as the order of magnitude of the tolerance of solver which was set to 10^{-9} [47]. In other words, *all the linearization schemes*

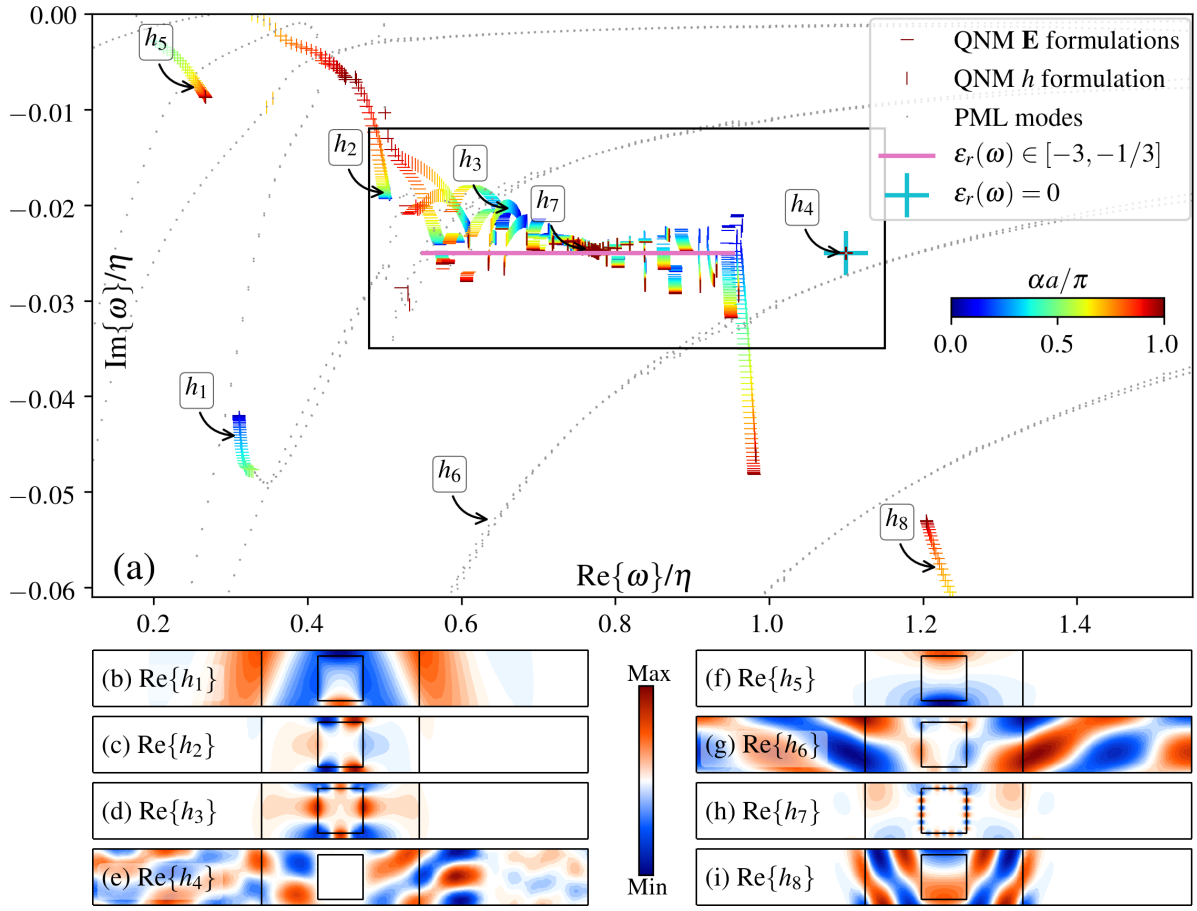

Figure 3: Dispersion relation of the grating in the complex frequency plane. The reduced Brillouin zone is spanned by α in color scale from 0 to π/a with 60 points. All electric field formulations (Aux-E, PEP-E, NEP-E, Lag-E) give identical eigenvalues up to the solver tolerance and are represented by hyphens "_". The magnetic field formulation PEP-h is represented by vertical hyphens "|". The critical interval of complex frequencies due to sharp corners is represented by the pink solid line. The large blue plus represents the relevant zero of $\varepsilon_{r,1}$.

presented for the electric field are numerically equivalent. The magnetic field formulation PEP-h fits the other cases with good accuracy outside the black rectangular frame.

Now let us look into the differences between the electric and magnetic field formulations, wherever horizontal and vertical bars do not form a "+") by recalling the properties of three particular regions [25] of the complex plane: ω such that $\varepsilon_{r,1}(\omega) \in [-I_\theta, -1/I_\theta]$, $\varepsilon_{r,1}(\omega) = 0$, and $\varepsilon_{r,1}(\omega) \to \infty$.

6.2 Corner modes and surface plasmons: $\varepsilon_{r,1}(\omega) \in [-I_\theta, -1/I_\theta]$

In recent works, variational formulations of the Helmholtz equation with sign changing coefficients has drawn a lot of attention in both direct [48, 49] and spectral problems [50]. The sesquilinear form involving the sign-changing coefficient becomes non coercive and one cannot use the Lax-Milgram theorem to establish well-posedness. In the direct problem, with a real and fixed frequency, the problem exists but it is hidden by the simple fact that most of physical problems are dissipative (*i.e.* the real-part changing coefficient has a non vanishing imaginary part). However, in spectral problems with *complex frequencies*, one can always find regions of

the complex plane of frequencies for which the *sign-changing coefficient is purely real.*

One important starting point is that it is possible to foresee [50] the critical complex frequencies: Given a sharp angle θ of the considered object with negative permittivity, the problem is ill-posed for:

$$\varepsilon_{r,1} \in [-I_\theta, -1/I_\theta], \text{ where } I_\theta = \max\left(\frac{2\pi-\theta}{\theta}, \frac{\theta}{2\pi-\theta}\right). \tag{27}$$

In this case, singularities appear at the corners and the expected corner modes are becoming more and more oscillating in the close vicinity of the corner. These solutions are no longer of finite energy, so in the functional frame of classical Galerkin FE used here, these modes known as "black-hole waves" cannot be represented. It is interesting to note that corner modes correspond to continuous spectrum just as free-space. This corner problem is a generalization of the well known one occurring at flat interfaces ($\theta = \pi$). The critical interval reduces then to the singleton $\{-1\}$.

Following the meshing prescriptions in Refs. [48, 49], *a structured symmetric mesh is imposed at each sign-changing interface and corner* (cf. Fig. 2, Fig. 4(d) and Fig. 6). As clearly illustrated in Appendix II (cf. Fig. 6) in the case of a simple planar slab, using an arbitrary unstructured mesh around a sign-changing interface leads to a highly unstable numerical discretization of the plasmonic accumulation point.

For the present dispersive rod consisting of $\pi/2$ angles, the critical interval is $[-3, -1/3]$. When applying the Drude model to complex frequencies, the quadratic equation $\varepsilon_{r,1}(\omega_c) = \kappa$ has one root ω_c in the quarter complex plane of interest for any $\kappa \in [-3, -1/3]$: $\omega_c = -i\gamma_d/2 + \sqrt{-\gamma_d^2/4 + \omega_d^2/(1-\kappa)}$.

The thick purple segment in Figs. 3 shows the locus of ω_c as κ spans $[-3, -1/3]$. In other words, all the eigenvalues around this segment correspond to corner modes. This explains the shift between the edge-based (electric) discretizations and the nodal (magnetic) one: *They both fail at capturing the corner effect in a different manner.* Indeed, in the (in-plane) edge case, the relevant unknowns associated with the corner are the circulation of the field along the two adjacent edges discretizing the corner, whereas in the (out-of-plane) nodal case, one unknown lies exactly on the corner. As moving closer to the critical interval, one finds higher order surface modes with rapid spatial frequencies (see eigenvector h_2, h_3 and finally h_7 in Fig. 3(c,d,h)), to finally find in the vicinity of $\omega/\varepsilon_{r,1}(\omega) = -1$ undersampled eigenvectors appearing as four weighted hot spots around each corner of the square.

An interesting and rigorous workaround could consist in using a special kind of PML dedicated to corners [51]. To the best of our knowledge, this type of PML has never been implemented to compute spectra of dispersive and lossy materials and it is a separate subject of study. More pragmatically, it is tempting to reduce the critical interval by slightly rounding the corners. In Appendix II, the effect of a rounding on only one mesh element is shown to be quite spectacular. Even with rounded corners, an accumulation point of eigenvalues [25] cannot be avoided at the plasmon frequency such that $\varepsilon_{r,1}(\omega) = -1$. It corresponds to all surface plasmon modes supported around the rod, with spatial variations tending towards infinity (cf. Appendix II).

Note that the spectrum of the original square structure is modified by both the corner PML (by selecting an outgoing wave condition at the corner) and the rounded geometry (obviously).

6.3 Divergence failure: $\varepsilon_{r,1}(\omega) = 0$

The second type of particular point corresponds to the zeros of the dispersive permittivity $\varepsilon_{r,1}(\omega)$. With the Drude model, the region of interest exhibits a single zero shown in Fig. 3(a) by a large blue "+". When reaching a zero of $\varepsilon_{r,1}$, the divergence condition $\mathrm{div}(\boldsymbol{\varepsilon}_r \mathbf{E}) = 0$ fails to give information about the electric field $\mathbf{E}$ which acquires supplemental degrees of freedom. For the 60 EVPs solved to compute the dispersion relation, an average number of 130 eigenvalues out of the 500 computed correspond to zeros of the permittivity. It is of course a limitation in terms of computation time. Note that these points are trivial to compute so that a numerical workaround would consist in adding some exclusion regions of the complex plane thanks to the SLEPc region class. This problem does not occur in the s-pol case, where the only unknown is E_z, since 2D nodal elements are divergence free by construction ($\partial_x E_x = \partial_y E_y = \partial_z E_z = 0$). A reason for solving the p-pol case using the PEP-h was to check whether the impact of this problem could be reduced using the magnetic field. It is not the case, since the average number of eigenvalues found at $\omega/\varepsilon_{r,1} = 0$ is about 130 (out of 500) for electric field formulations and 135 for PEP-h. Looking at the particular eigenvector labelled h_4 in Fig. 3(e), the field appears constant inside the dispersive rod and exhibits random fluctuations outside. One possible workaround consists in enforcing the appropriate divergence condition by adjunction of a Lagrange multiplier.

6.4 Bulk accumulation point: $\varepsilon_{r,1}(\omega) \to \infty$

The eigenvectors associated with eigenvalues found around the poles of the eigenvalue-dependent permittivity present no characteristic spatial variations since they can be arbitrarily rapid. For a Drude model, poles are 0 and $-i\gamma$. It was chosen to avoid these points using the rectangular region provided by SLEPc. Indeed, eigenfrequencies with null real parts are usually not relevant. However, when considering a permittivity model with poles in the region of interest (*e.g.* a Lorentz model), it is of prime importance to take this accumulation point into account as we already evidenced in [52].

6.5 Convergence

Even away from the critical interval, it is legitimate to question the convergence of the eigenvalues. Let us focus on one eigenvalue in particular, the lowest (fundamental) eigenfrequency for $\alpha = 3\pi/(4a)$, denoted $\omega^\diamond$. It corresponds to the lowest frequency band shown in Fig. 3(f). Figure 4(b) shows the value of $|\omega^\diamond|$ as a function of the mesh refinement. For 100 mesh elements per period, 5 significant digits are found on the real part and 6 on the imaginary part.

The convergence rate of this eigenvalue with the mesh refinement is shown in Fig. 4(a). The numerical value of this eigenfrequency for a mesh size parametrized by N is denoted $\omega_N^\diamond$ and the quantity $\big||\omega_N^\diamond| - |\omega_{N-2}^\diamond|\big|$ is represented as a function of N, from $N = 7$ to $N = 100$ for interpolation orders 1 and 2. All the formulations are represented with the following color code : PEP-h in purple (FE order 1) and green (FE order 2), electric field formulations in orange (FE order 1) and blue (FE order 2). Again, it is stressed that the eigenvalues $\omega_N^\diamond$ shown in Fig. 4(a) are identical up to the solver tolerance irrespectively of the electric field formulation and in spite of the different treatment of the non-linearity leading to the discrete systems (except for the PEP-E and NEP-E cases which share the very same FE matrices).

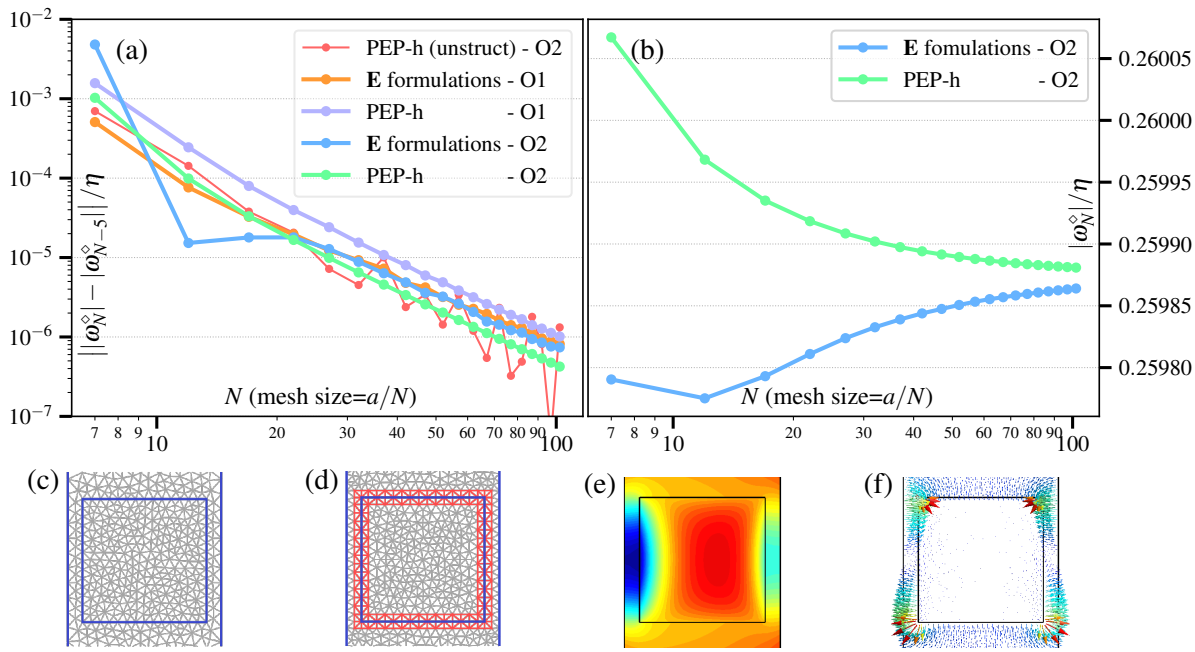

Figure 4: (a) Convergence rate of an eigenvalue of $\omega^\diamond$ as a function of the mesh size parametrized by N for electric and magnetic formulations and two FE orders. (b) $|\omega_N^\diamond|$ as a function of N (c) Unstructured mesh sample . (d) Structured mesh sample . (e) Real part of the scalar mode $h^\diamond$ corresponding to $\omega^\diamond$. (f) Real part of the vector mode $\mathbf{E}^\diamond$ corresponding to $\omega^\diamond$.

With the classical unstructured Delaunay mesh (see Fig. 4(c)), an erratic behavior is obtained (see the thin red line in Fig. 4(a)) which is consistent with the results in [48, 51].

The corresponding modes profiles $h^\diamond$ (obtained with nodal elements and the PEP-h approach) and $\mathbf{E}^\diamond$ (obtained with edge elements and the NEP-E approach) are depicted in Fig. 4(e) and Fig. 4(f) respectively. It is clear from this last figure that the hot spots at the corners play an important role in the convergence, even though $\omega^\diamond$ is away from the critical interval. It can explain the absence of the expected change of slope [40] in the convergence rate when increasing the polynomial order of the FE shape functions: The solution at corners is not regular enough to be significantly improved by higher orders.

6.6 Computation time and memory requirements

Some computation details are given for the most time consuming simulations presented in this paper used to produce Figs. 3(a) with $N = 8$ and second order FE. These simulations ran on a machine equipped with Intel Xeon 2.7GHz processors. First, the RAM memory used is linked to both the system size and the SLEPc solver used. The most memory and time consuming approach is the auxiliary field one. The extra volume unknowns increase the system size by one third compared to the PEP/NEP-E approaches. Note that there is one single auxiliary field in this Drude case. The average computation times for one value of the Bloch variable are, by descending order, 10m18s (Aux-E, 44596 DOFs, 2.8Gb memory), 9m45s (Lag-E, 34750 DOFs, 2.6Gb memory), 9m30s (PEP-E, 34150 DOFs, 2.6Gb memory), 8m49s (NEP-E, 34150 DOFs, 1.5Gb memory), 5m13s (PEP-h, 23688 DOFs, 2.3Gb memory). The computation times follows unsurprisingly the number of degrees of freedom and the sparsity of the matrices. Note that the approach using SLEPc non-linear rational NLEIGS solver is the fastest for this problem

Table 2: A synthetic view of strengths and weaknesses of all the presented approaches.

Approach	Advantage	Limitation
Aux-E	• Physical linearization • Low polynomial order (2) • Easy to extend to several materials with more poles	• System size • Speed
PEP-E	• Smallest system size	• Tedious to generalize • Polynomial order with several materials
NEP-E	• Smallest system size • Memory footprint • Shortest runtime • Ease of implementation	• Stability and convergence with several materials?
Lag-E	• Domain by domain formulation with extra boundary unknowns • Low polynomial order	• Extra boundary unknowns
PEP-h	• For comparison purposes, especially around the critical interval	• 2D scalar case only

among vector formulations, faster than PEP-E, due to its smaller memory footprint.

Finally, with a reasonably fine mesh ($N = 6$), it is stressed that the provided model that retrieves the eigenvalue $\omega^\diamond$ runs within a few seconds on any laptop.

7 Conclusion

In this paper, we have presented a framework to solve non-linear eigenvalue problems suitable for a Finite Element discretization. The implementation is based on the open-source FE software GetDP and the open-source library SLEPc.

Several approaches aimed at the linearization of the eigenvalue problem arising from the consideration of frequency-dispersion in electromagnetic structures have been introduced, implemented and discussed. The relative permittivity was considered under the form of a rational function of the eigenvalue with arbitrary degrees for the denominator and numerator. Five formulations were derived in the frame of a typical multi-domain problem exhibiting several key features in electromagnetism: The mono-dimensional grating is a quasi-periodic problem with PMLs. This is a 2D problem quite representative of 3D situations since the physics is as rich as in 3D (exhibiting surface plasmons) and the vector case with edge elements is tackled. We take advantage of the performance and versatility of the SLEPc library whose non-linear eigenvalue solvers were interfaced with the flexible GetDP FE GNU software for the purpose of this study. An open-source template model based on the ONELAB interface to Gmsh/GetDP is provided and can be freely downloaded from [24]. It exhibits the various ways to set up non-linear EVPs in the newly introduced GetDP syntax: One rational EVP and four polynomial EVPs with various degrees are shown.

The first four formulations of the 2D grating problem concern the vector case and the choice of unknown is the electric field. First, physical auxiliary fields (Aux-E) allow to linearize of the problem by extending Maxwell's operator. The unknowns are added in the dispersive domains solely. The final polynomial EVP is quadratic. Second, writing the Maxwell problem

under its variational form brings out a rational (NEP-E) and a polynomial (PEP-E) eigenvalue problem. An alternative consists in dealing with the rational function under the strong form of the problem and making the use of Lagrange multipliers (Lag-E) to deal with the non-classical boundary terms arising from this formulation. The advantage of this approach is to keep the order of the polynomial EVP as small as possible. Finally, for comparison, the polynomial approach is given for the scalar version of same polarization case using the magnetic field (PEP-h).

We obtain a perfect numerical agreement between all the electric field approaches in spite of the fact that they rely on very different linearization strategies. As for the magnetic one, when away from the critical interval inherent to the presence of the sign changing permittivity and sharp angles, the agreement still holds. As for this critical interval associated with solutions of infinite energy, they cannot be captured with a classical FE scheme. Specific PMLs could be adapted. However, away from the critical interval, for instance for the fundamental mode of the grating, a smooth convergence is obtained when using a specific locally structured and symmetric mesh.

To conclude on the main features of the presented approaches, the SLEPc rational NLEIGS solver used in the NEP-E approach gives the best results in terms of ease of implementation, speed, and memory occupation in this test case with a simple Drude model. In spite of its much larger size than with all other approaches, the auxiliary fields approach is very valuable for validation purposes since it relies on a very different linearization mechanism and thus completely different sparse matrices. The approach using Lagrange multipliers (Lag-E) deserves some attention since the polynomial order will not blow up with an increased number of dispersive materials. Finally, for this problem involving the permittivity directly given as a rational function, the NEP-E approach should be preferred over the PEP-E one.

Direct perspectives of this work consist in applying these different approaches to the 3D case with more sophisticated permittivity functions. But considering several distinct materials, relying on permittivity functions with more poles, implies the presence of more complicated frequency lines in the complex plane leading to additional critical intervals. Inevitably, special treatments should be investigated for the corners issue.

Appendix I A standard representation of the dispersion relation

A standard representation of the dispersion relation for gratings is shown in Fig. 5 using the very same numerical data as in Fig. 3. This figure shows $\mathrm{Re}\{\omega\}$ against α, while $\mathrm{Im}\{\omega\}$ is given in color scale.

The modes of the continuum (or free space modes or PML modes) corresponding to radiation losses are shown in grey symbols for both formulations. Two criteria are used to classify these modes as PML modes. The other modes are considered as QNMs of the grating. The first criterion relies on the independence of the QNM towards the PML parametrization. The dispersion relation has been computed twice with two different values of the complex coordinate stretch parameter s_y (1+i and 1+2i) defined in Eq. (7). The eigenvalues whose both real and imaginary parts change by less than 1% between the two computations are kept and fed to the next criterion. Indeed the first stability criterion is sufficient for an isolated scatterer surrounded by a PML: A single branch of continuous spectrum is rotated around the origin by an angle of $\mathrm{Arg}\{s_y\}/2$. However, in periodic cases, several PML branches are obtained in the

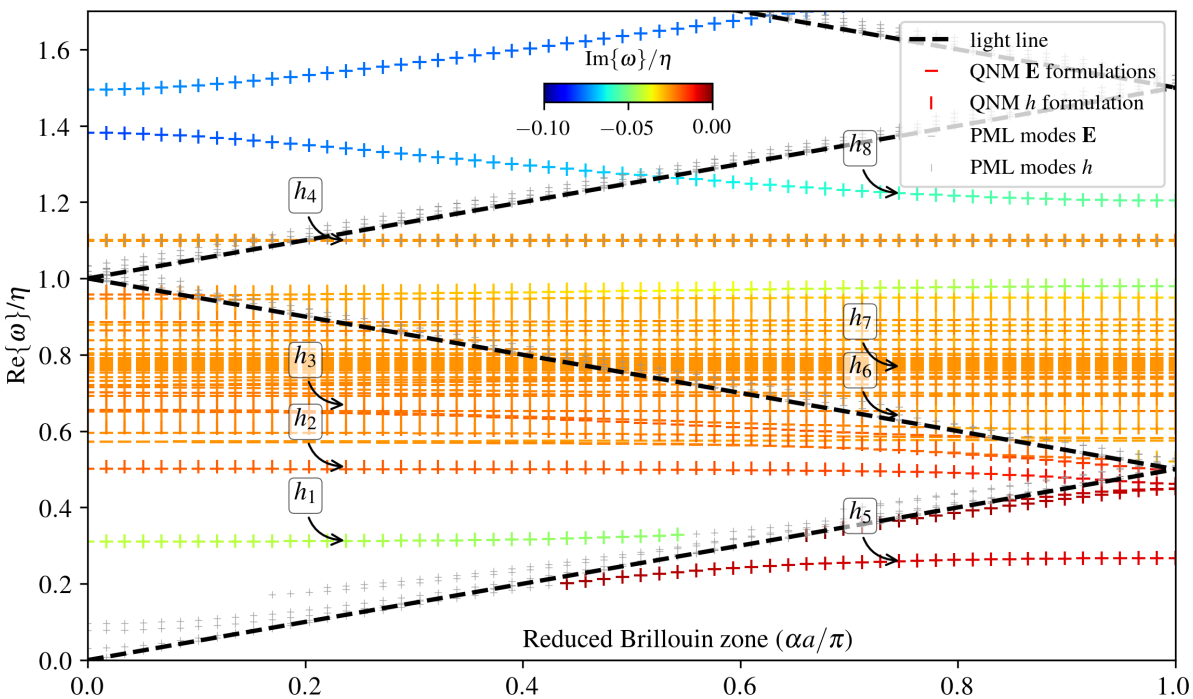

Figure 5: (a) Real (ordinate axis) and imaginary parts (jet color scale) of the normalized eigenvalues ($\eta = \frac{2\pi c}{a}$) as a function of the Bloch variable α for the five methods. Electric (resp. magnetic) field formulations are represented by hyphens "_" (resp. vertical hyphens "|"). The folded light line is depicted as a black dashed line.

frequency range of interest, which corresponds to the fact that the structure interacts with the continuum through its infinite set of diffraction orders [27]. These branches rotate by an angle of $\mathrm{Arg}\{s_y\}/2$ around the points sitting at $n\pi/a$ on the real line, where n is an integer. As a consequence, all the PML modes close to these points on the real line are not discarded by the first criterion above. The second criterion relies on the fact that eigenvectors corresponding to PML modes are mostly located into the PMLs as shown in Fig. 3(g). The second criterion classifies as PML mode an eigenvector h_n satisfying $\int_{\Omega_1^d \cup \Omega_2^\varnothing} |h_n| \, \mathrm{d}\Omega / \int_{\Omega_1^\varnothing \cup \Omega_3^\varnothing} |h_n| \, \mathrm{d}\Omega > 0.5$. Note that the threshold values of 1% for the first criterion and 0.5 for the second criterion depend on the mesh refinement and PML thicknesses respectively. Modes which do not fall into the two categories defined above are considered as QNMs and represented by colored vertical hyphens (PEP-h) and horizontal hyphens (electric field cases) in Fig. 5.

Just below the first branch of the folded light line represented by the dashed black line, the shape of the band corresponding to the lowest eigenfrequency supported by the grating is characteristic of the fundamental mode of this type of structure [53, 54, 55, 46]. The real part of an eigenfield of this particular band (h_5) is shown in Fig. 3(g). Other higher bands appear below the first branch of the folded light line for higher values of the Bloch wavevector α. After the first folding of the light line at $\mathrm{Re}\{\omega\}/\eta \approx 0.45$, classical bands are retrieved but some discrepancy appears between the electric formulations and the magnetic one as detailed in Sec. 6.1. The accumulation of flat bands in the range $0.55 < \mathrm{Re}\{\omega\}/\eta < 1.1$ corresponds to plasmons and corner modes. Finally, the dispersion relation retrieves a more conventional behavior, with very leaky higher frequency modes such as mode h_8 in Fig. 3(i).

Appendix II Structured meshes and rounding

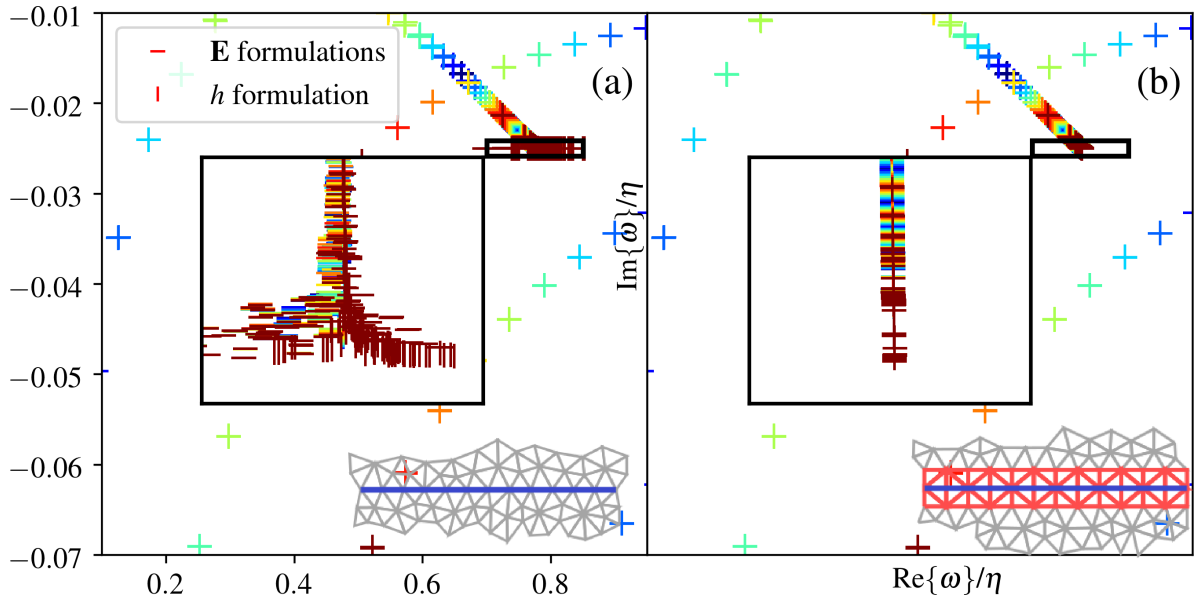

Figure 6: Spectrum of the slab in the complex plane calculated in 2D with a classical unstructured mesh (a) and with a structured mesh (b).

To illustrate the importance of imposing a symmetric mesh around a flat interface, the spectrum of a slab is depicted in Fig. 6. The slab is a 1D problem that can be treated here in 2D since it is trivially periodic (b=a). An accumulation point is expected at ω such that $\varepsilon_{r,1}(\omega) = -1$ (framed by a black rectangle in Figs. 6(a-b)). As can be noticed in the two insets, it is striking that the unstructured mesh leads to a poor description of the plasmonic accumulation point where the structured symmetric mesh preserves stability. The agreement between electric and magnetic formulations can be improved by slightly rounding the corners. The left panel of Fig. 7 corresponds to a zoom in the black frame of Fig. 3. The discrepancy is clearly visible. The right panel shows the spectrum of the slightly rounded square (the radius of the rounding is $a/25$, cf. mesh sample in the right inset). From the discrete point of view, four consecutive mesh edges of the mesh along the rounded corner form two by two angles of $3\pi/4$, which corresponds to a critical interval for $\varepsilon_{r,1}(\omega)$ of $[-1.66, -0.6]$ (pink line in the right panel). The agreement between the electric and magnetic formulations is now striking away from the reduced critical region (cf. hyphens "_" and "|" now forming "+" in the oval black frames).

Appendix III Implementation in GetDP

The GetDP software is an open source FE solver (`http://getdp.info`). It handles geometries and meshes generated using the open source mesh generator Gmsh (`http://gmsh.info`). The source codes of both softwares are available at `https://gitlab.onelab.info`.

A template model to allowing to retrieve the results of this paper is also available [24]. It relies on ONELAB, a lightweight interface between Gmsh and GetDP. To run the example, one can simply (i) download the precompiled binaries of Gmsh and GetDP available for all platforms

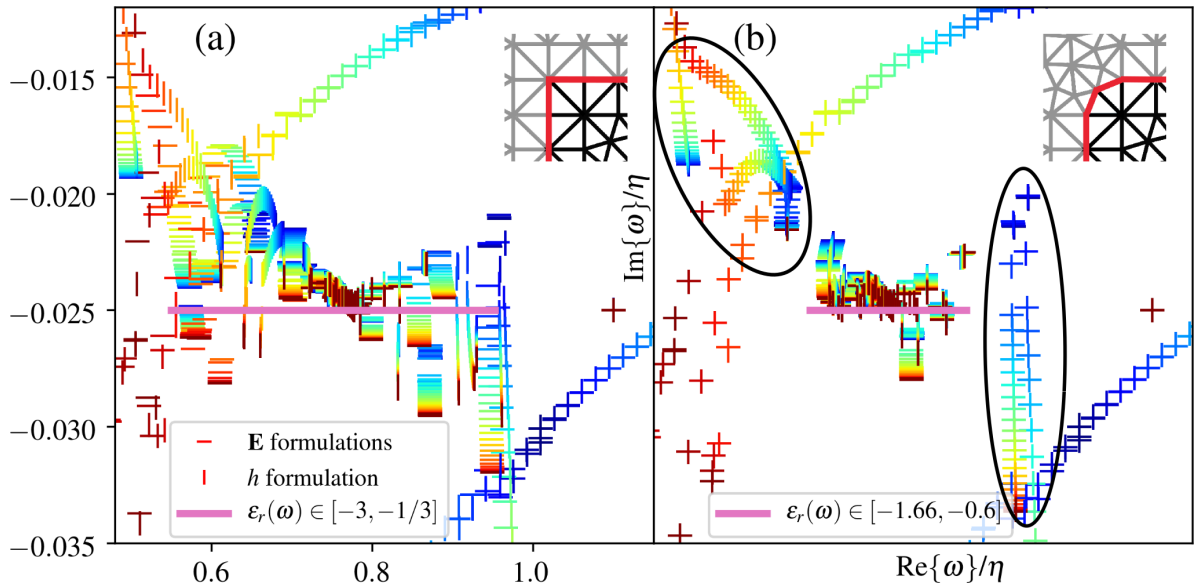

Figure 7: (a) Zoom in the black rectangle of Fig. 3(a). (b) Same result for a slight rounding of radius $a/25$ of all corners, *i.e.* a critical angle of $3\pi/4$ on three mesh nodes (see inset of the right pannel).

as a standalone ONELAB bundle from `http://onelab.info`, (ii) download the template model and (iii) open the `NonLinearEVP.pro` file with Gmsh.

This work has involved changes to GetDP in both the source code and the parser in order to call the relevant SLEPc solvers in a general manner. These changes now allow to solve a large class of non-linear (polynomial and rational) eigenvalue problems suitable for a FE discretization. Indeed, the software readily handles various FE basis functions relevant in electromagnetism, acoustics, elasticity... The example in electromagnetism in this paper has voluntarily been chosen relatively simple for the sake of clarity. As shown in Sec. 6.2 both the computation and the underlying physics of dispersive gratings modes are rather intricate.

In practice, a problem definition written in `.pro` input files is usually split between the objects defining data particular to a given problem, such as geometry, physical characteristics and boundary conditions (i.e., the `Group`, `Function` and `Constraint` objects), and those defining a resolution method, such as unknowns, equations and related objects (i.e., the `Jacobian`, `Integration`, `FunctionSpace`, `Formulation`, `Resolution` and `PostProcessing` objects). The processing cycle ends with the presentation of the results, using the `PostOperation` object.

The major changes appear at `Formulation` and `Resolution` stages. A new `Eig` operator was introduced in the parser. It can be invoked to set up a polynomial EVP when combined with the keyword `Order`, or a rational EVP when combined with the keyword `Rational`. The `Order` or `Rational` keywords allow to define the dependence of the problem with the eigenvalue $\lambda := i\omega$. Depending on whether `Order` or `Rational` is set, GetDP internally calls the static functions `_polynomialEVP` or `_nonlinearEVP` where the interface to SLEPc is written in practice. These functions can be found in the source code of GetDP in the C++ file `Kernel/EigenSolve_SLEPC.cpp` for further details.

Note that in all GetDP eigenvalue solvers the eigenvalue has been chosen to be $i\omega$, consistently with the convention in this paper. In the following GetDP listings, the dots (**...**) represent a deliberate omission of some instructions that are unnecessary to the comprehension of the implemented syntax. The reader is invited to refer to the template example to see these GetDP code snippets in their global context.

i Polynomial eigenvalue problems

Table 3: Correspondence between mathematical and GetDP objects.

GetDP object	Mathematical object	Description
`cel`	c	light celerity
`I[]`	i	$i^2 = -1$
`mur[]`	$\boldsymbol{\mu}_r(\mathbf{r})$	Tensor field
`epsr_nod[]`	$\boldsymbol{\varepsilon}_r^{\oslash}(\mathbf{r})$	Tensor field
`eps_oo_1`	ε_∞ (cf. Eq. (5a))	Flat contribution
`om_d_1`	ω_d (cf. Eq. (5a))	Plasma frequency
`gam_1`	γ_d (cf. Eq. (5a))	Damping frequency
`Om`	Ω	Computational domain
`Om_1`	Ω_1^d	Dispersive domain
`Om_2`	$\Omega^{\oslash}$	Non-dispersive domains
`Galerkin{ [ Dof{Curl u}, {Curl u}]; In Om ; ... }`	$+\int_\Omega \mathbf{curl}\,\mathbf{E} \cdot \overline{\mathbf{curl}\,\mathbf{W}}\,\mathrm{d}\Omega$	Contribution to the variational formulation
`Galerkin{ Eig[ Dof{u}, {u}]; Order 3 ; In Om_1 ; ... }`	$+\lambda^3 \int_{\Omega_d^1} \mathbf{E} \cdot \overline{\mathbf{W}}\,\mathrm{d}\Omega$	Contribution to the variational formulation in λ^3

GetDP now solves polynomial eigenvalue problems. Its syntax is shown in the listing 1. This GetDP formulation corresponds to the PEP-E formulation mathematically described in Eq. (20). For clarity, the correspondence between the relevant mathematical objects and GetDP objects are detailed in Table 3.

Listing 1: Syntax for the formulation of the polynomial eigenvalue problem. The dots (...) represent a deliberate ellipsis to the code.

```
{ Name pep; Type FemEquation;
  Quantity {
    { Name u ; Type Local; NameOfSpace Eedge;}
  }
  Equation {
    Galerkin{   [-cel^2/mur[]*gam_1*Dof{Curl u},{Curl u}];           In Om   ; ...}
    Galerkin{Eig[ cel^2/mur[]       *Dof{Curl u},{Curl u}]; Order 1; In Om   ; ...}
    Galerkin{Eig[ om_d_1^2          *Dof{u}     ,{u}     ]; Order 1; In Om_1; ...}
    Galerkin{Eig[-eps_oo_1*gam_1    *Dof{u}     ,{u}     ]; Order 2; In Om_1; ...}
    Galerkin{Eig[ eps_oo_1          *Dof{u}     ,{u}     ]; Order 3; In Om_1; ...}
    Galerkin{Eig[-epsr_nod[]*gam_1  *Dof{u}     ,{u}     ]; Order 2; In Om_2; ...}
    Galerkin{Eig[ epsr_nod[]        *Dof{u}     ,{u}     ]; Order 3; In Om_2; ...}
  }
}
```

Note that the PEP-h formulation involves a 4th order polynomial eigenvalue problem, and the Aux-E formulation involves a quadratic one.

ii Rational non-linear eigenvalue problems

GetDP now solves rational eigenvalue problems. Its syntax is shown in Listing 2. This GetDP formulation corresponds to the NEP-E formulation mathematically described in Eq. (19).

Listing 2: Syntax for the formulation of the rational eigenvalue problem. The dots (...) represent a deliberate ellipsis to the code.

```
{ Name form_nep; Type FemEquation;
  Quantity {
    { Name u ; Type Local; NameOfSpace Eedge;}
  }
  Equation {
      Galerkin{Eig[ cel^2/mur[]*Dof{Curl u}, {Curl u} ]; Rational 1; In Om   ; ... }
      Galerkin{Eig[-epsr_nod[] *Dof{u}     , {u}      ]; Rational 2; In Om_1; ... }
      Galerkin{Eig[-epsr_nod[] *Dof{u}     , {u}      ]; Rational 3; In Om_2; ... }
  }
}
```

Then, at the `Resolution` step, each rational function expected as a factor of each `Galerkin` term is specified. The 6th (respectively 7th) argument of the `EigenSolve` function is a list of polynomial numerators (resp. denominators), each polynomial numerator (resp. denominator) being itself given as a list of GetDP floats. The position of each numerator (resp. denominator) in the list of numerators (resp. denominators) corresponds to the tag following the `Rational` keyword. A polynomial numerator (resp. denominator), is represented by a list of (real) floats by decreasing power of λ. For instance, the list `-eps_oo_1,gam_1*eps_oo_1,-om_d_1^2,0` in Listing 3 represents the polynomial $-\varepsilon_\infty\lambda^3+\gamma_d\varepsilon_\infty\lambda^2-\omega_d^2\lambda$, numerator of $\lambda^2\varepsilon_{r,1}(\lambda)$. Likewise, the list `1,-gam_1` in Listing 3 represents the polynomial $\lambda-\gamma_d$, denominator of $\lambda^2\varepsilon_{r,1}(\lambda)$. Note that the degrees of the numerators and denominators can be arbitrarily large.

Listing 3: Syntax for the resolution of the rational eigenvalue problem

```
{ Name res_nep;
  System{{ Name M; NameOfFormulation form_nep; Type ComplexValue;}}
  Operation{
    GenerateSeparate[M1];
    EigenSolve[M,neig,target_real,target_imag,EigFilter[],
      {{1}, {-eps_oo_1,gam_1*eps_oo_1, -om_d_1^2,0}, {-1,0,0}} ,
      {{1}, {1,-gam_1},                              {1}     } ];
  }
}
```

iii Specifying the eigensolver

The general SLEPc options for solving of non-linear problems are preset in the source code of GetDP (see `Kernel/EigenSolve_SLEPC.cpp`). Additional or alternative SLEPc options can be passed as command line argument when calling GetDP. There are particularly relevant options that can be passed to SLEPc:

- **Target**: SLEPc eigensolvers will return `nev` eigenvalues closest to a given target value. The `nev` parameter can be specified by the user (1 by default), as well as the target value, that represents a point in the complex plane around which the eigenvalues of interest are located. The values can be provided via the ONELAB dialog boxes of the provided open-source model, or alternatively with the command line arguments `-pep_nev` (or `-nep_nev`), and `-pep_target` (or `-nep_target`).

- **Regions**: The eigenvalues are returned sorted according to their distance to the target. However, only eigenvalues lying inside the region of interest are returned (in other words, eigenvalues outside the region of interest are discarded). The region of interest (which is a rectangle by default) can be specified by the user via the ONELAB dialog boxes of the provided open-source model, or alternatively with the command line argument `-rg_interval_endpoints` (or any other options related to region specification, see SLEPc documentation [47] for details).

iv Generalization

With the change made to GetDP, one can tackle much more general problems. For instance, if the geometry has N dispersive materials with distinct material dispersion, one would just need to extend the recipe above, as schematized in the GetDP Listing 4. Note that a numerator or denominator can be provided as a GetDP list directly, defined in the `Function` object.

Listing 4: Syntax for a general problem with several dispersive materials

```
{ Name form_nep; Type FemEquation;
  Quantity {
    { Name u ; Type Local; NameOfSpace Eedge;}
  }
  Equation {
    Galerkin { Eig[   1/mur[] *    Dof{Curl u}, {Curl u} ]; Rational 1; In Om  ; ... }
```

```
    Galerkin { Eig[ -epsr_nod[]/cel^2 * Dof{u}, {u}      ]; Rational 2; In Om_1; ... }
    Galerkin { Eig[ -epsr_nod[]/cel^2 * Dof{u}, {u}      ]; Rational 3; In Om_2; ... }
    Galerkin { Eig[ -epsr_nod[]/cel^2 * Dof{u}, {u}      ]; Rational 4; In Om_3; ... }
    Galerkin { Eig[ -epsr_nod[]/cel^2 * Dof{u}, {u}      ]; Rational 5; In Om_4; ... }
    ...
  }
}
...
{ Name res_nep;
  System{{ Name M; NameOfFormulation form_nep; Type ComplexValue;}}
  Operation{
    GenerateSeparate[M1];
    EigenSolve[M,neig,target_real,target_imag,EigFilter[],
               {num_1(), num_2(), num_3(), num_4(), num_5(), ... }
               {den_1(), den_2(), den_3(), den_4(), den_5(), ... }];
  }
}
```


Acknowledgements

The work was partly supported by the French National Agency for Research (ANR) under the project "Resonance" (ANR-16-CE24-0013). The authors acknowledge the members of the project "Resonance" for fruitful discussions. C. Campos and J. E. Roman were supported by the Spanish Agencia Estatal de Investigación (AEI) under project SLEPc-HS (TIN2016-75985-P), which includes European Commission ERDF funds. C. Geuzaine was supported by ARC grant for Concerted Research Actions (ARC WAVES 15/19-03), financed by the Wallonia-Brussels Federation of Belgium.

The authors thank Christian Engström from Umeå Universitet for helpful comments. Maxence Cassier from Institut Fresnel is acknowledged. Finally, the authors address special thanks to Anne-Sophie Bonnet Ben-Dhia and Camille Carvalho from INRIA (POEMS) for their motivating remarks and insights.

References

[1] T. Betcke, N. J. Higham, V. Mehrmann, C. Schröder, and F. Tisseur, "Nlevp: A collection of nonlinear eigenvalue problems," *ACM Transactions on Mathematical Software (TOMS)*, vol. 39, no. 2, p. 7, 2013.

[2] J. D. Jackson, *Classical electrodynamics*. John Wiley & Sons, 2007.

[3] M. G. Silveirinha, "Metamaterial homogenization approach with application to the characterization of microstructured composites with negative parameters," *Physical Review B*, vol. 75, no. 11, p. 115104, 2007.

[4] A. Alu, "First-principles homogenization theory for periodic metamaterials," *Physical Review B*, vol. 84, no. 7, p. 075153, 2011.

[5] Y. Liu, S. Guenneau, and B. Gralak, "Causality and passivity properties of effective parameters of electromagnetic multilayered structures," *Physical Review B*, vol. 88, no. 16, p. 165104, 2013.

[6] P. G. Etchegoin, E. Le Ru, and M. Meyer, "An analytic model for the optical properties of gold," *The Journal of Chemical Physics*, vol. 125, no. 16, p. 164705, 2006.

[7] M. Garcia-Vergara, G. Demésy, and F. Zolla, "Extracting an accurate model for permittivity from experimental data: hunting complex poles from the real line," *Optics Letters*, vol. 42, no. 6, pp. 1145–1148, 2017.

[8] C. Sauvan, J.-P. Hugonin, I. Maksymov, and P. Lalanne, "Theory of the spontaneous optical emission of nanosize photonic and plasmon resonators," *Physical Review Letters*, vol. 110, no. 23, p. 237401, 2013.

[9] B. Vial, M. Commandré, G. Demésy, A. Nicolet, F. Zolla, F. Bedu, H. Dallaporta, S. Tisserand, and L. Roux, "Transmission enhancement through square coaxial aperture arrays in metallic film: when leaky modes filter infrared light for multispectral imaging," *Opt. Lett.*, vol. 39, pp. 4723–4726, Aug 2014.

[10] W. Yan, R. Faggiani, and P. Lalanne, "Rigorous modal analysis of plasmonic nanoresonators," *Physical Review B*, vol. 97, no. 20, p. 205422, 2018.

[11] P. Lalanne, W. Yan, K. Vynck, C. Sauvan, and J.-P. Hugonin, "Light interaction with photonic and plasmonic resonances," *Laser & Photonics Reviews*, vol. 12, no. 5, p. 1700113, 2018.

[12] H. van der Lem, A. Tip, and A. Moroz, "Band structure of absorptive two-dimensional photonic crystals," *JOSA B*, vol. 20, no. 6, pp. 1334–1341, 2003.

[13] Q. Bai, M. Perrin, C. Sauvan, J.-P. Hugonin, and P. Lalanne, "Efficient and intuitive method for the analysis of light scattering by a resonant nanostructure," *Optics express*, vol. 21, no. 22, pp. 27371–27382, 2013.

[14] T. Weiss, M. Mesch, M. Schäferling, H. Giessen, W. Langbein, and E. Muljarov, "From dark to bright: first-order perturbation theory with analytical mode normalization for plasmonic nanoantenna arrays applied to refractive index sensing," *Physical review letters*, vol. 116, no. 23, p. 237401, 2016.

[15] J. Zimmerling, L. Wei, P. Urbach, and R. Remis, "A Lanczos model-order reduction technique to efficiently simulate electromagnetic wave propagation in dispersive media," *Journal of Computational Physics*, vol. 315, pp. 348–362, 2016.

[16] J. Zimmerling, L. Wei, P. Urbach, and R. Remis, "Efficient computation of the spontaneous decay rate of arbitrarily shaped 3D nanosized resonators: a Krylov model-order reduction approach," *Applied Physics A*, vol. 122, no. 3, p. 158, 2016.

[17] D. A. Powell, "Resonant dynamics of arbitrarily shaped meta-atoms," *Physical Review B*, vol. 90, no. 7, p. 075108, 2014.

[18] D. A. Powell, "Interference between the modes of an all-dielectric meta-atom," *Physical Review Applied*, vol. 7, no. 3, p. 034006, 2017.

[19] F. Tisseur and K. Meerbergen, "The quadratic eigenvalue problem," *SIAM Review*, vol. 43, no. 2, pp. 235–286, 2001.

[20] D. S. Mackey, N. Mackey, and F. Tisseur, "Polynomial eigenvalue problems: theory, computation, and structure," in *Numerical Algebra, Matrix Theory, Differential-Algebraic Equations and Control Theory* (P. Benner *et al.*, eds.), pp. 319–348, 2015.

[21] S. Güttel and F. Tisseur, "The nonlinear eigenvalue problem," *Acta Numerica*, vol. 26, pp. 1–94, 2017.

[22] V. Hernandez, J. E. Roman, and V. Vidal, "SLEPc: A scalable and flexible toolkit for the solution of eigenvalue problems," *ACM Transactions on Mathematical Software*, vol. 31, no. 3, pp. 351–362, 2005.

[23] P. Dular, C. Geuzaine, F. Henrotte, and W. Legros, "A general environment for the treatment of discrete problems and its application to the finite element method," *IEEE Transactions on Magnetics*, vol. 34, no. 5, pp. 3395–3398, 1998.

[24] G. Demésy, 2018.

[25] Y. Brûlé, B. Gralak, and G. Demésy, "Calculation and analysis of the complex band structure of dispersive and dissipative two-dimensional photonic crystals," *JOSA B*, vol. 33, no. 4, pp. 691–702, 2016.

[26] F. Teixeira and W. Chew, "Systematic derivation of anisotropic pml absorbing media in cylindrical and spherical coordinates," *IEEE microwave and guided wave letters*, vol. 7, no. 11, pp. 371–373, 1997.

[27] B. Vial, F. Zolla, A. Nicolet, and M. Commandré, "Quasimodal expansion of electromagnetic fields in open two-dimensional structures," *Physical Review A*, vol. 89, p. 023829, Feb. 2014.

[28] A. Bermúdez, L. Hervella-Nieto, A. Prieto, R. Rodri, *et al.*, "An optimal Perfectly Matched Layer with unbounded absorbing function for time-harmonic acoustic scattering problems," *Journal of Computational Physics*, vol. 223, no. 2, pp. 469–488, 2007.

[29] A. Modave, E. Delhez, and C. Geuzaine, "Optimizing Perfectly Matched Layers in discrete contexts," *International Journal for Numerical Methods in Engineering*, vol. 99, no. 6, pp. 410–437, 2014.

[30] F. Zolla, G. Renversez, A. Nicolet, B. Kuhlmey, S. Guenneau, and D. Felbacq, *Foundations of photonic crystal fibres.* World Scientific, 2005.

[31] A. Tip, "Linear absorptive dielectrics," *Physical Review A*, vol. 57, no. 6, p. 4818, 1998.

[32] B. Gralak and A. Tip, "Macroscopic Maxwell's equations and negative index materials," *Journal of Mathematical Physics*, vol. 51, no. 5, p. 052902, 2010.

[33] A. Tip, "Some mathematical properties of Maxwell's equations for macroscopic dielectrics," *Journal of Mathematical Physics*, vol. 47, no. 1, p. 012902, 2006.

[34] A. Raman and S. Fan, "Photonic band structure of dispersive metamaterials formulated as a Hermitian eigenvalue problem," *Physical Review Letters*, vol. 104, no. 8, p. 087401, 2010.

[35] A. Taflove and S. C. Hagness, *Computational electrodynamics: the finite-difference time-domain method.* Artech house, 2005.

[36] A. Nicolet, S. Guenneau, C. Geuzaine, and F. Zolla, "Modelling of electromagnetic waves in periodic media with finite elements," *Journal of Computational and Applied Mathematics*, vol. 168, no. 1, pp. 321–329, 2004.

[37] P. Monk *et al.*, *Finite element methods for Maxwell's equations*. Oxford University Press, 2003.

[38] C. Geuzaine and J.-F. Remacle, "Gmsh: a three-dimensional finite element mesh generator with built-in pre- and post-processing facilities," *International Journal for Numerical Methods in Engineering*, vol. 79, no. 11, pp. 1309–1331, 2009.

[39] J. Webb and B. Forgahani, "Hierarchal scalar and vector tetrahedra," *IEEE Transactions on Magnetics*, vol. 29, no. 2, pp. 1495–1498, 1993.

[40] C. Geuzaine, B. Meys, P. Dular, and W. Legros, "Convergence of high order curl-conforming finite elements [for EM field calculations]," *IEEE Transactions on Magnetics*, vol. 35, no. 3, pp. 1442–1445, 1999.

[41] "ONELAB website," 2018.

[42] D. Lu, Y. Su, and Z. Bai, "Stability analysis of the two-level orthogonal Arnoldi procedure," *SIAM Journal on Matrix Analysis and Applications*, vol. 37, no. 1, pp. 195–214, 2016.

[43] C. Campos and J. E. Roman, "Parallel Krylov solvers for the polynomial eigenvalue problem in SLEPc," *SIAM Journal on Scientific Computing*, vol. 38, no. 5, pp. S385–S411, 2016.

[44] C. Campos and J. E. Roman, "NEP: a module for the parallel solution of nonlinear eigenvalue problems in SLEPc," `arXiv:1910.11712`, 2019.

[45] S. Güttel, R. van Beeumen, K. Meerbergen, and W. Michiels, "NLEIGS: A class of fully rational Krylov methods for nonlinear eigenvalue problems," *SIAM Journal on Scientific Computing*, vol. 36, no. 6, pp. A2842–A2864, 2014.

[46] P. Lalanne, W. Yan, A. Gras, C. Sauvan, J.-P. Hugonin, M. Besbes, G. Demésy, M. Truong, B. Gralak, F. Zolla, *et al.*, "Quasinormal mode solvers for resonators with dispersive materials," *JOSA A*, vol. 36, no. 4, pp. 686–704, 2019.

[47] J. E. Roman, C. Campos, E. Romero, and A. Tomas, "SLEPc users manual," Tech. Rep. DSIC-II/24/02 - Revision 3.9, D. Sistemes Informàtics i Computació, Universitat Politècnica de València, 2018.

[48] L. Chesnel and P. Ciarlet, "T-coercivity and continuous Galerkin methods: application to transmission problems with sign changing coefficients," *Numerische Mathematik*, vol. 124, no. 1, pp. 1–29, 2013.

[49] A.-S. Bonnet-Ben Dhia, C. Carvalho, and P. Ciarlet, "Mesh requirements for the finite element approximation of problems with sign-changing coefficients," *Numerische Mathematik*, vol. 138, pp. 801–838, Apr 2018.

[50] C. Carvalho, L. Chesnel, and P. Ciarlet, "Eigenvalue problems with sign-changing coefficients," *Comptes Rendus Mathematique*, 2017.

[51] C. Carvalho, *Étude mathématique et numérique de structures plasmoniques avec coins*. PhD thesis, ENSTA ParisTech, 2015.

[52] F. Zolla, A. Nicolet, and G. Demésy, "Photonics in highly dispersive media: the exact modal expansion," *Optics letters*, vol. 43, no. 23, pp. 5813–5816, 2018.

[53] P. Lalanne, J. Rodier, and J. Hugonin, "Surface plasmons of metallic surfaces perforated by nanohole arrays," *Journal of Optics A: Pure and Applied Optics*, vol. 7, no. 8, p. 422, 2005.

[54] P. Lalanne, J. P. Hugonin, and P. Chavel, "Optical properties of deep lamellar gratings: a coupled Bloch-mode insight," *Journal of Lightwave Technology*, vol. 24, no. 6, pp. 2442–2449, 2006.

[55] G. Schider, J. Krenn, A. Hohenau, H. Ditlbacher, A. Leitner, F. Aussenegg, W. Schaich, I. Puscasu, B. Monacelli, and G. Boreman, "Plasmon dispersion relation of Au and Ag nanowires," *Physical Review B*, vol. 68, no. 15, p. 155427, 2003.